Experimental Evaluation of Honeycomb/Screen Configurations and Short Contraction Section for NASA Lewis Research Center's Altitude Wind Tunnel

Richard R. Burley and
Douglas E. Harrington

NASA

Experimental Evaluation of Honeycomb/Screen Configurations and Short Contraction Section for NASA Lewis Research Center's Altitude Wind Tunnel

Richard R. Burley and
Douglas E. Harrington

*Lewis Research Center
Cleveland, Ohio*

Summary

An experimental investigation was conducted in the high-speed leg of the 0.1-scale model of the proposed Altitude Wind Tunnel to evaluate several flow conditioner configurations in the settling chamber at tunnel Mach numbers from 0.20 to 0.916. How honeycomb/screen axial location in the settling chamber affected the flow in the upstream part of the contraction section was also investigated. Turbulence intensity in the octagonal test section was estimated from measured values at the contraction-section entrance.

The lowest longitudinal turbulence intensity measured at the contraction-section entrance was 1.2 percent. It was achieved with a configuration consisting of a honeycomb plus three fine-mesh screens. Turbulence intensity in the test section was estimated to be between 0.1 and 0.2 percent with the honeycomb plus three fine-mesh screens in the settling chamber. Adding screens adversely affected the total pressure profile, causing a small total pressure defect near the centerline of the contraction-section entrance. The wall surface Mach number distribution in the upstream part of the contraction section was essentially unaffected by the axial location of the honeycomb/screen configuration. No significant boundary layer separation was evident throughout the entire length of the short contraction section.

Introduction

It has been proposed that the NASA Lewis Research Center rehabilitate and extend the capabilities of its Altitude Wind Tunnel (AWT) to meet the aeropropulsion needs of the next century. The AWT (fig. 1) was first brought on line in 1944 and was used for aeropropulsion research until 1958, when it was converted into a series of altitude test chambers for space research. As originally configured, the AWT had a maximum Mach number of 0.6 at an altitude of 9100 m (30 000 ft) with total temperature capability down to −38 °C (−36 °F). Because all the internal components were removed in the conversion, the proposed AWT would require all new internal components.

The planned rehabilitated tunnel (fig. 2) would have an expanded Mach number capability of 0.9+, altitude pressures up to 16 800 m (55 000 ft), and total temperature capability down to −51 °C (−60 °F). New capabilities would include adverse-weather test environments (icing, freezing rain, heavy rain, and snow) and acoustical instrumentation in the test section. The settling chamber, located in the large-diameter return circuit, where the velocity is low, would contain a honeycomb and screens to straighten the flow and reduce its turbulence between the exit of corner 4 and the entrance to the contraction section. The contraction section would then accelerate the flow and further reduce its turbulence so that the desired conditions could be achieved in the test section. The test section would be octagonal in cross section with a 6.1-m (20-ft) span across the flats. The test-section walls would be acoustically treated, slotted, and surrounded by a 12.2-m (40-ft) diameter plenum tank tied into a plenum evacuation system (PES) to provide for high-quality test-section airflow with high-blockage models. The proposed rehabilitated AWT is described more completely in references 1 to 4.

Because of the magnitude of the AWT rehabilitation and the significant extensions to its original capability, a modeling program (both experimental and analytical) comprising several 0.1-scale models was undertaken to ensure the technical soundness of the new component designs. The 0.1-scale model size was selected because of facility modeling experience at this scale (refs. 5 and 6) and because it represented the upper limit of the exhaust flow capability available at Lewis for providing model airflow.

Experimental results concerning some components of the modeling program have been reported. Reference 7 presents preliminary findings and progress in the modeling program. References 8 to 11 present results on the new turning vanes. Reference 12 presents the Mach number distributions on the walls of the octagonal test section.

The present investigation concerned additional components of the modeling program and had four objectives: (1) to evaluate how various honeycomb/screen configurations in the settling chamber affected the longitudinal turbulence intensity and the uniformity of the total pressure profile at the contraction-section entrance; (2) to determine the total pressure loss across the flow conditioners; (3) to determine how honeycomb/screen axial location in the settling chamber affected the flow in the upstream part of the contraction section; and (4) to estimate the longitudinal turbulence intensity in the octagonal test section. These objectives were achieved in the high-speed leg of the tunnel, which consisted of the tunnel settling chamber, the contraction section, the slotted test section of 11-percent open area surrounded by the PES, and the high-speed diffuser. An engine exhaust scoop, planned for the full-scale AWT (fig. 2), was not installed for this phase of testing.
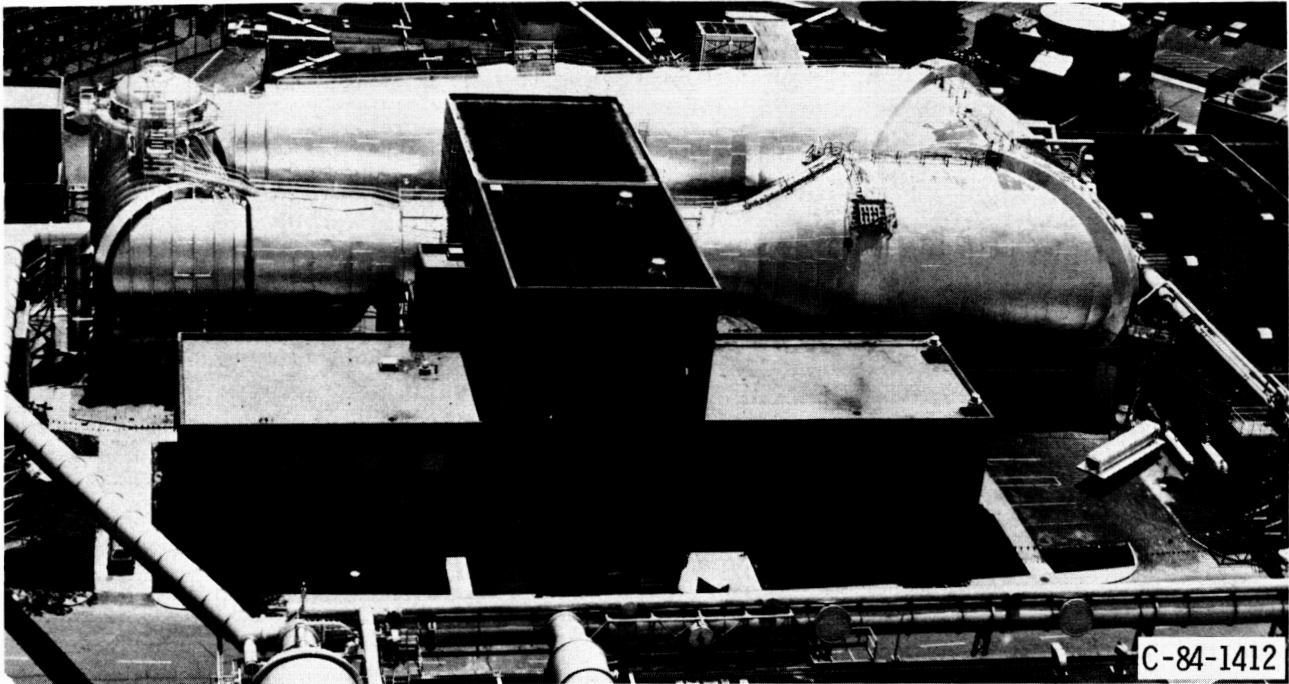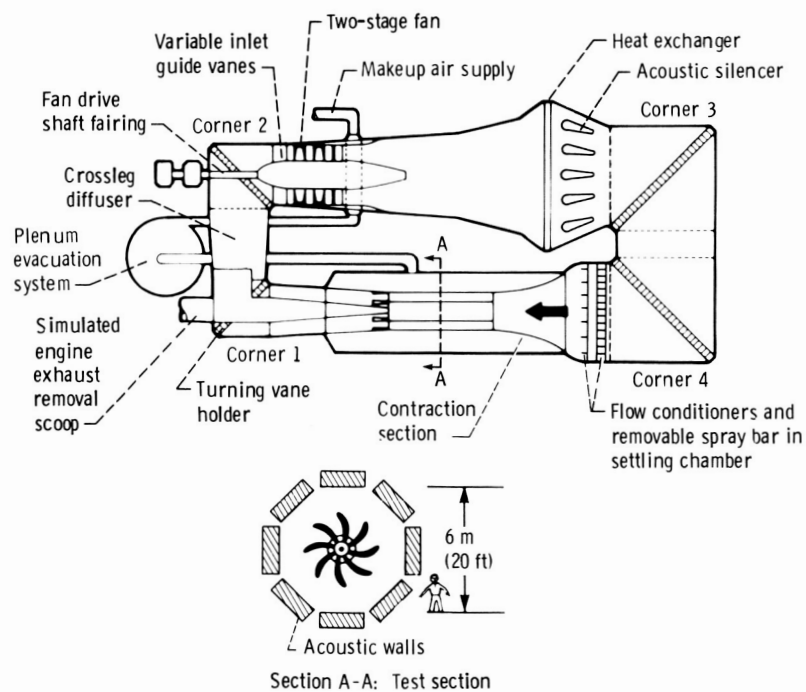
Figure 1.—Exterior configuration of the Lewis Research Center's Altitude Wind Tunnel.

Section A-A: Test section

Mach number	0 to 0.9+
Altitude, m (ft)	0 to 16 800 (0 to 55 000)
Total temperature, $^{\circ}$C ($^{\circ}$F)	-51 to 15.5 (-60 to 60)
Test-section acoustic level, dB (OASPL)	120

Figure 2.—Capabilities of modified and rehabilitated Altitude Wind Tunnel.

Symbols

A cross-sectional area, cm^2 (in.^{2})

D diameter, cm (in.)

L length, cm (in.)

M Mach number

P total pressure, N/cm^2 (psi)

$\bar{P}$ area-averaged total pressure, N/cm^2 (psi)

q dynamic pressure, N/cm^2 (psi)

R radius, cm (in.)

U mean velocity in longitudinal direction, m/sec (ft/sec)

u' rms velocity fluctuation in longitudinal direction, m/sec (ft sec)

V area-averaged velocity in longitudinal direction, m/sec (ft/sec)

x axial distance, cm (in.)

θ circumferential location, deg

Subscripts:

cs contraction section

max   maximum

sc settling chamber

ss spool section

ts test section

w wall

Apparatus and Procedure

Test Apparatus

The test apparatus (figs. 3 and 4) was a 0.1-scale model of the high-speed leg proposed for the Lewis Altitude Wind Tunnel (AWT). It modeled the settling chamber, contraction section, test section, and diffuser section proposed for the modified AWT.

Geometric details of the facility are shown in figure 5. Dry air, supplied by the Lewis central air supply system, entered the tunnel through a 76-cm (30-in.) diameter supply pipe. The supply pipe, which extended well into the plenum tank, was perforated and had a series of baffles attached at right angles to its vertical centerline. The plenum tank internal walls were acoustically treated with Kevlar. The plenum tank had an internal diameter of 243.8 cm (96 in.) and was 421 cm (166 in.) long. The downstream end of the tank had provisions for different screen and grid configurations.

Immediately downstream of the screens was a bellmouth that reduced the internal diameter to 155.5 cm (61.2 in.). The diameter then remained constant for a length of 102 cm
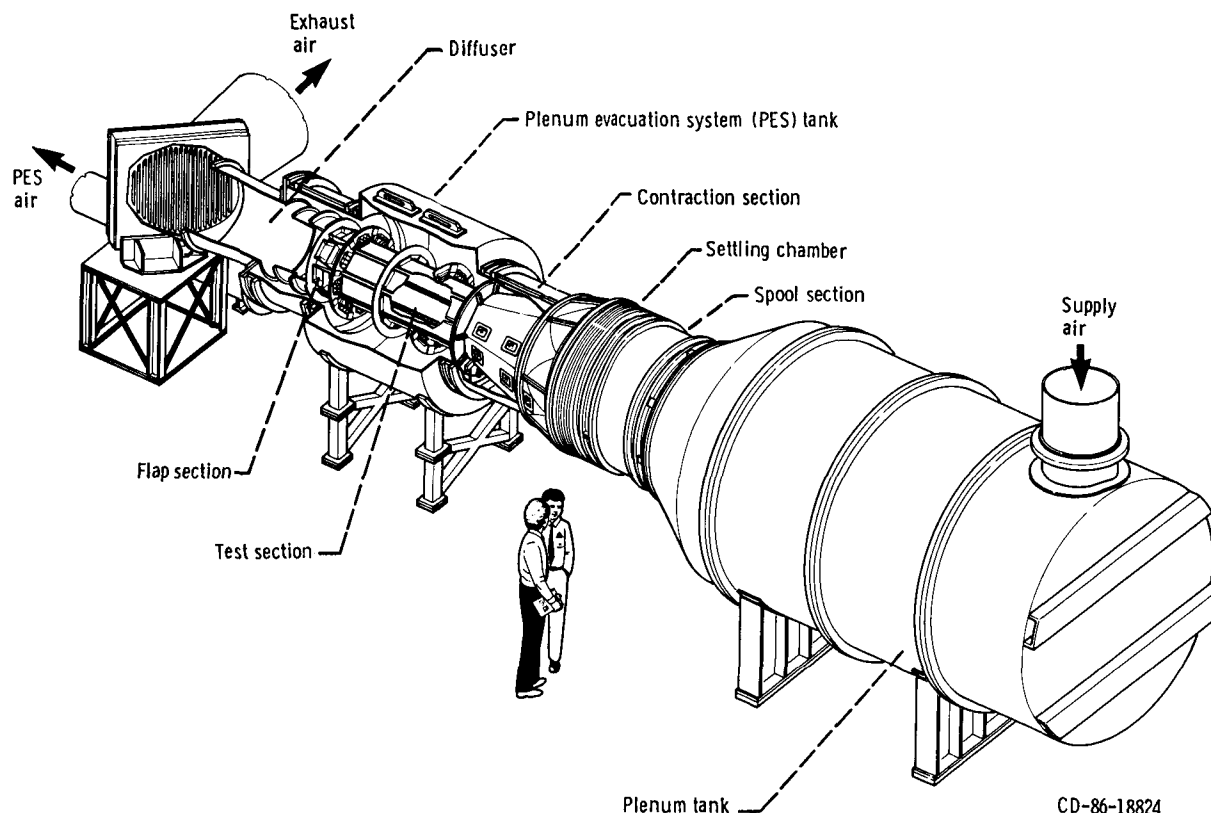

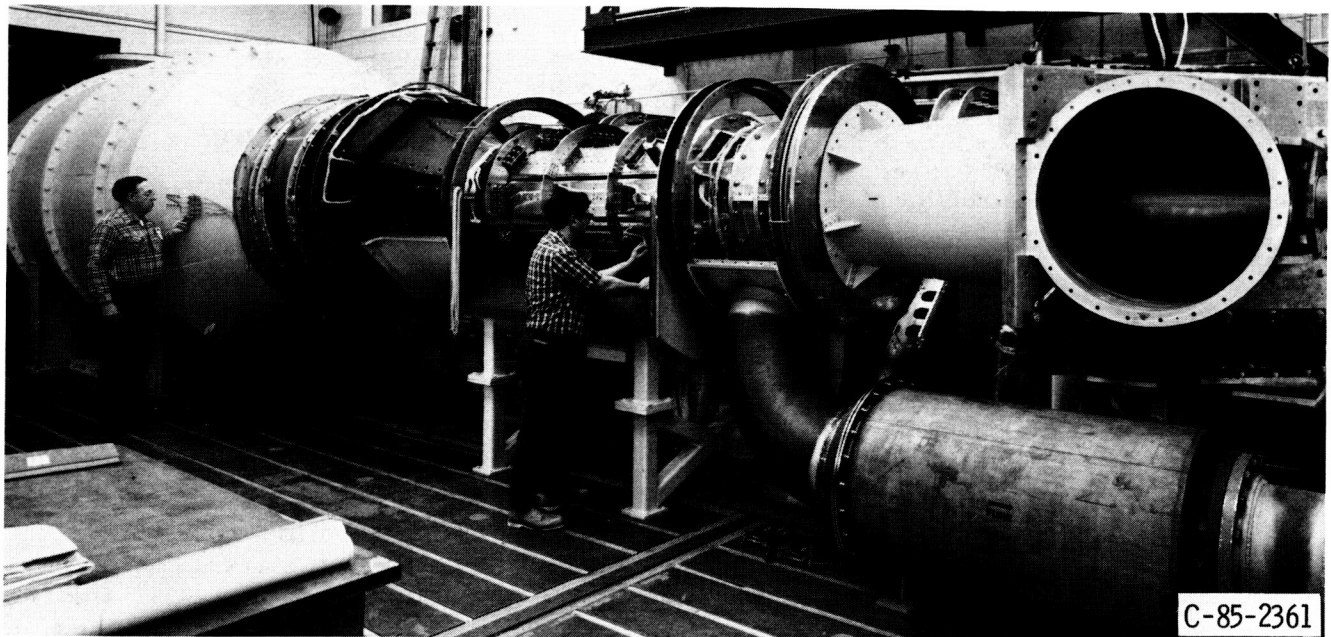Figure 3.—Schematic of test apparatus.

CD-86-18824

C-85-2361

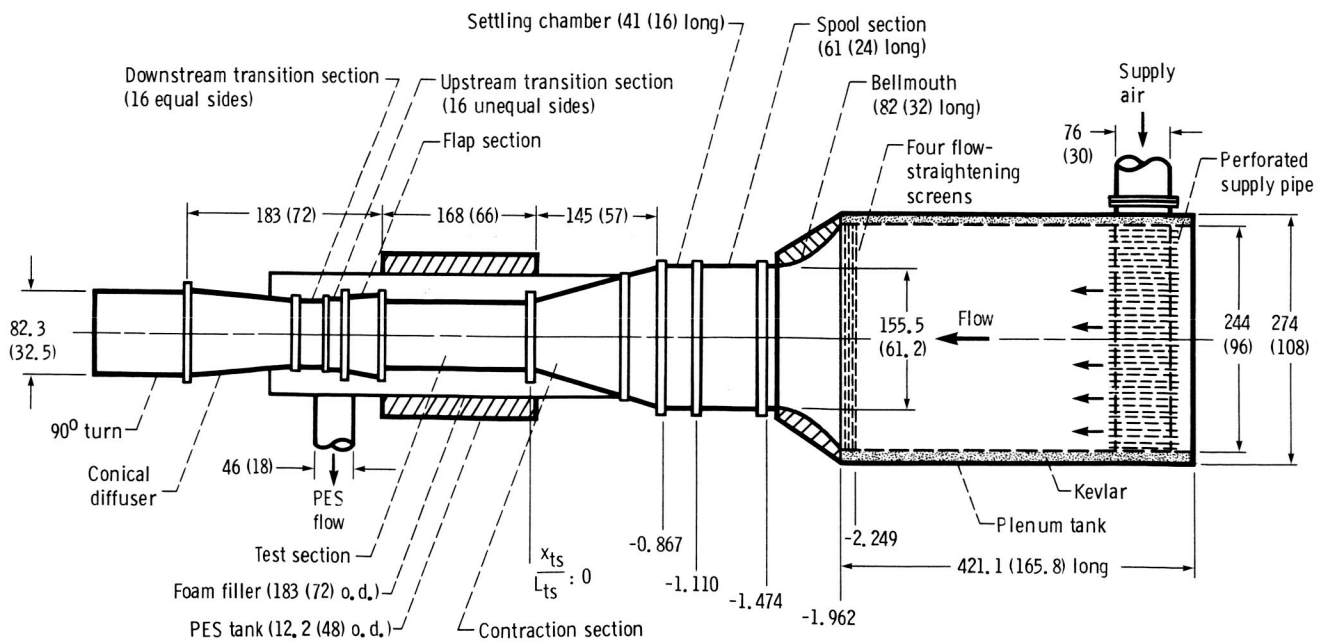Figure 4.—Test facility (as seen from other side).

Figure 5.—Geometric details of test apparatus (elevation). (All dimensions are in centimeters (inches).)

(40 in.). This constant-diameter section, which included a 61-cm (24-in.) long spool section followed by a 40.7-cm (16-in.) long settling chamber, was designed to hold a variety of flow-conditioning devices. A number of combinations of honeycomb, screens, and grids were tested in the settling chamber. The spool section was not part of the 0.1-scale model of the AWT. It was installed for the present investigation to improve the uniformity of the velocity profile exiting the bellmouth in order to achieve as uniform a velocity profile as possible entering the settling chamber.

Downstream of the settling chamber was the contraction section. It transitioned from a circular cross section that matched the settling chamber to an octagonal cross section that matched the test section. The contraction ratio, which was 6.503 with a length-to-maximum-diameter ratio of 0.935, was rather small for the amount of area reduction. The values of contraction ratio and length-to-diameter ratio resulted from constraints imposed by the existing structure of the AWT. Five small windows were located in the contraction walls (fig. 3) to allow television cameras to view the tufts attached to the contraction-section walls.

Downstream of the contraction section was the octagonal, slotted 168-cm (66-in.) long test section. Test-section open area could be varied. For the present test the open area was 11 percent.

Following the test section was a diffuser 183 cm (72 in.) long with a half-angle of 3°. It included a flap section, an upstream transition section, a downstream transition section, and a conical diffuser (fig. 6). The flaps could be positioned at any angle from 0° to 9° as shown in figure 7. For the present test the flaps were positioned at 0°. Previous tests (ref. 12) showed that the flap position did not significantly affect

Figure 6.—Major components of diffuser including flap section and two transition sections (looking upstream).

pressures near the start of the test section over the entire range of tunnel Mach numbers examined. Consequently the flap position would not be expected to have any effect on pressures upstream of the test section.

The test section and parts of the contraction section and diffuser were enclosed in a large plenum chamber (figs. 3 to 5). During tunnel operation the plenum evacuation system (PES) flow could be exhausted through a 45.7-m (18-in.) diameter exhaust line to Lewis' altitude exhaust system. The PES, the diffuser, and the test section are described more completely in reference 12.

Instrumentation

Tunnel mass flow rate was measured with a standard ASME sharp-edge orifice plate. Orifice temperatures were measured with copper-constantan thermocouples; orifice pressures were measured with individual transducers. Tunnel flow rates ranged from approximately 21 kg/sec (46 lbm/sec) at a tunnel Mach number of 0.20 to 67 kg/sec (147 lbm/sec) at a tunnel Mach number of 0.916. PES flow rate was zero. Previous tests (ref. 12) showed that PES flow rates up to 3 percent of the tunnel flow rate did not significantly affect pressures near the start of the test section over the entire range of tunnel Mach numbers examined. Consequently changes in the PES flow would not be expected to have any effect on pressures upstream of the test section.

Pressure and temperature instrumentation at the entrance to the spool section ($x_{ts}/L_{ts} = -1.474$) is shown in figure 8. The total pressure at the spool-section entrance was obtained from the arithmetic average of the four pressures at the innermost radial location ($R/R_{cs} = 0.877$) on the rakes. During initial testing it was determined that this value of total pressure was the same as that obtained from an area-weighted average of 32 pressures measured on two rakes 90° apart that spanned the entrance to the spool section. Total temperature was obtained from the arithmetic average of the four Chromel-Alumel thermocouples at $R/R_{cs} = 0.910$ on the rakes. Static pressure was obtained from the arithmetic average of all 16 static pressures on the outer wall.

Pressure and temperature instrumentation near the contraction-section entrance ($x_{ts}/L_{ts} = -0.851$) is shown in figure 9. Total pressure was obtained from the area-weighted average of all 32 pressures on the rakes. Total temperature was obtained from the arithmetic average of all 16 Chromel-Alumel thermocouples on the rakes. Static pressure was obtained from the arithmetic average of all 16 static pressures on the outer wall. The J1 to J4 information shown in figure 9(a) will be used in some subsequent figures to indicate circumferential location of the total pressure rakes.

All pressures except orifice pressures were measured with an electronically scanned pressure system. The system consisted of a number of modules, each of which contained 32 individual transducers. Total and static pressures at the entrances to the spool section ($x_{ts}/L_{ts} = -1.474$) and the
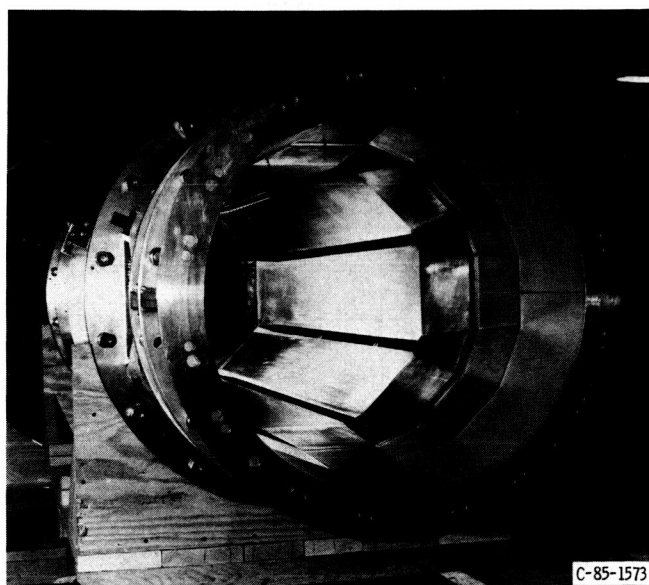
Section A-A

Flap-section entrance $(x_{ts}/L_{ts} = 1.0)$
(looking downstream)
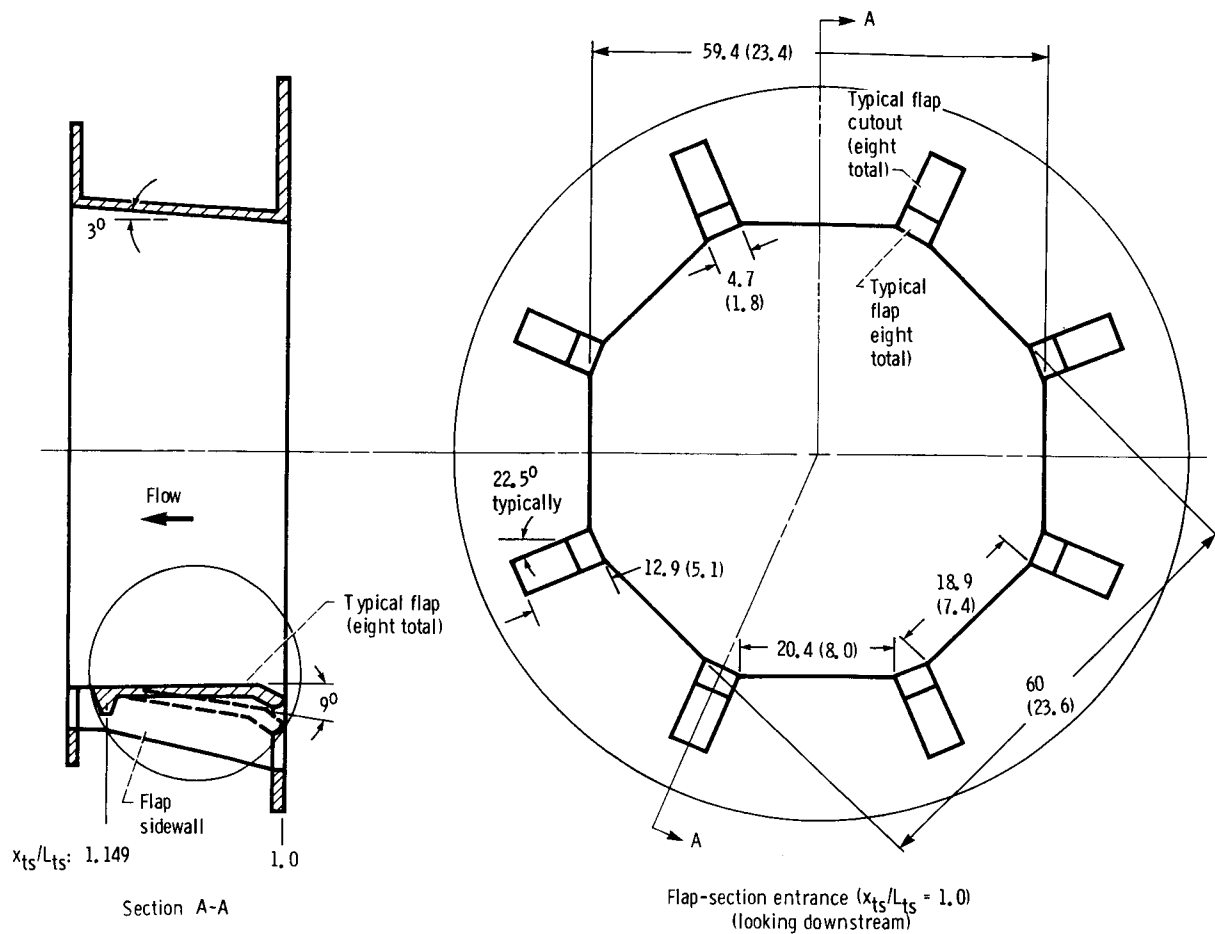
Figure 7.—Geometric details of flap section. (All dimensions are in centimeters (inches).)

o Total pressure probe
● Static pressure tap
● Thermocouple

Probe	Radial location R/R_{ss}
1	0.877
2	.910
3	.935
4	.951
5	.967
6	.984

Looking upstream

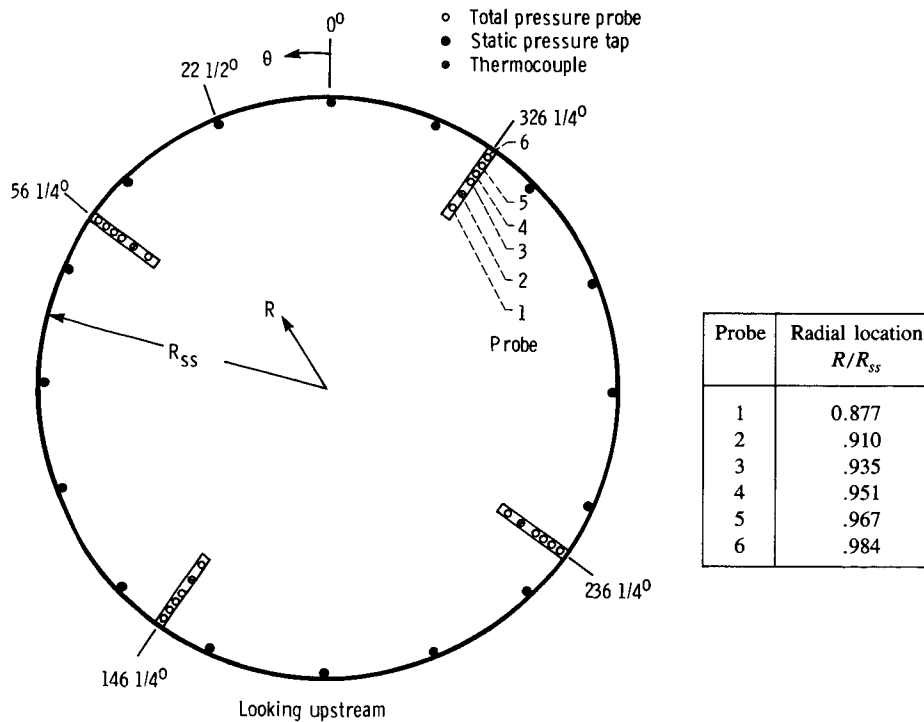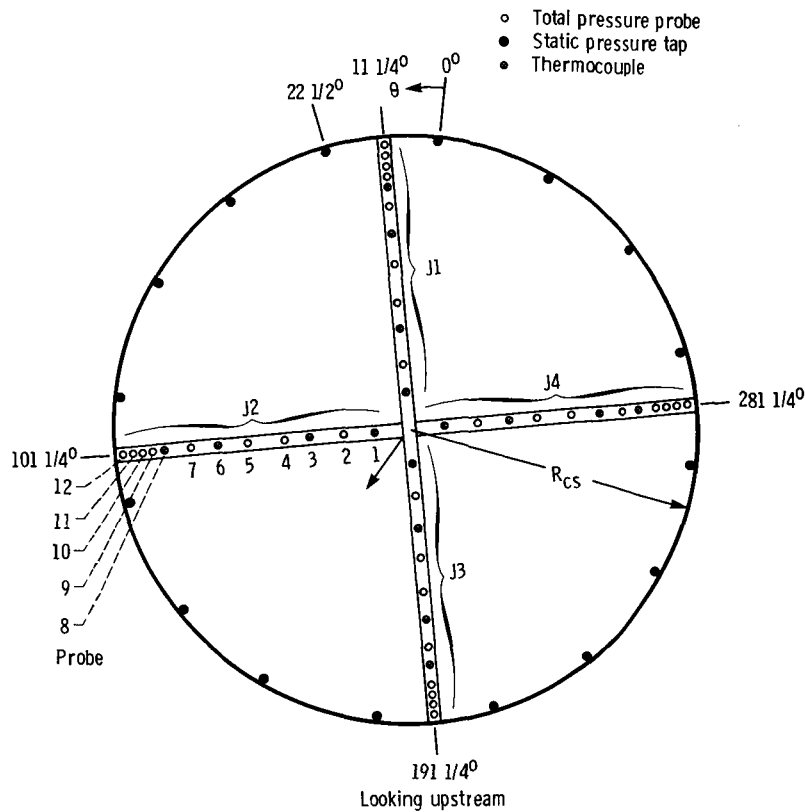Figure 8.—Pressure and temperature instrumentation at entrance to test section $(x_{ts}/L_{ts} = -1.474)$.

Figure 9.—Pressure and temperature instrumentation at entrance to contraction section $(x_{ts}/L_{ts} = -0.851)$.

Probe	Radial location R/R_{cs}
1	0.065
2	.125
3	.316
4	.376
5	.626
6	.692
7	.877
8	.910
9	.935
10	.951
11	.967
12	.984

contraction section $(x_{ts}/L_{ts} = -0.851)$ were measured with ± 34.5-kN/m^2 (± 5-psid) transducers having an accuracy of ± 0.048 kN/m^2 (± 0.007 psi). The remaining pressures, consisting mostly of contraction-section static pressures, were measured with ± 103.4-kN/m^2 (± 15-psid) transducers having an accuracy of ± 0.138 kN/m^2 (± 0.02 psi).

Four hot-wire probes (fig. 10) were positioned at the entrance to the contraction section 90° apart at a radial location $R/R_{cs} = 0.614$. This location was dictated by the length of the available probes. Each probe held a single-wire tungsten element calibrated over the range of velocities that would be encountered in the settling chamber. The 0.00038-cm (0.00015-in.) diameter, 0.127-cm (0.050-in.) long wires were positioned with their long axis normal to the flow to measure turbulence in the axial direction.

All the hot-wire anemometers (fig. 11) were operated in the constant-temperature mode. Hot-wire voltage was monitored on an oscilloscope. Also, the voltage was split into its rms and dc components and each was recorded on the data-recording system. Standard hot-wire equations for incompressible flow (e.g., ref. 13) were used to calculate axial turbulence.

Thirty-nine static pressure taps were located at each of seven circumferential locations on the internal walls of the contraction section (fig. 12). Because the flow was assumed to be symmetrical about the horizontal centerline, only the upper half of the contraction section was instrumented. The circumferential locations were chosen so that, in the octagonal
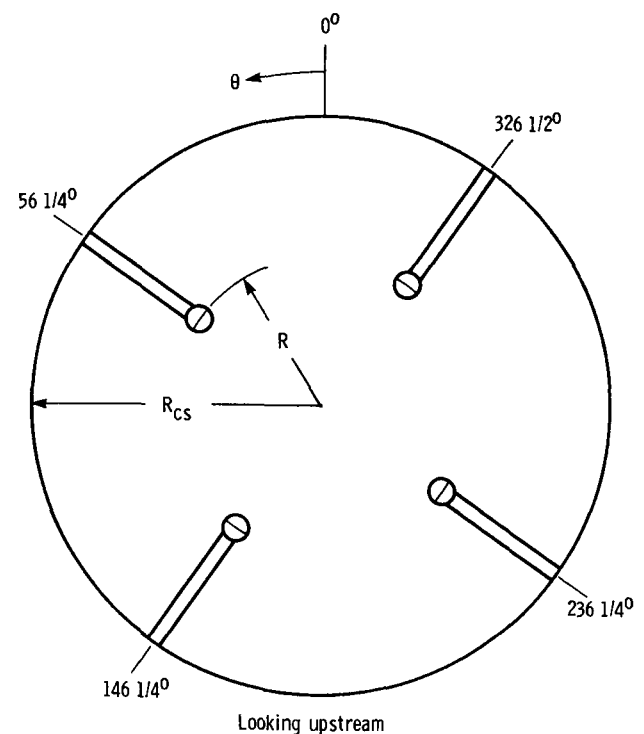

Figure 10.—Hot-wire probes at entrance to contraction section $(x_{ts}/L_{ts} = -0.851)$. Radius of contraction section, $R/R_{cs} = 0.614$.
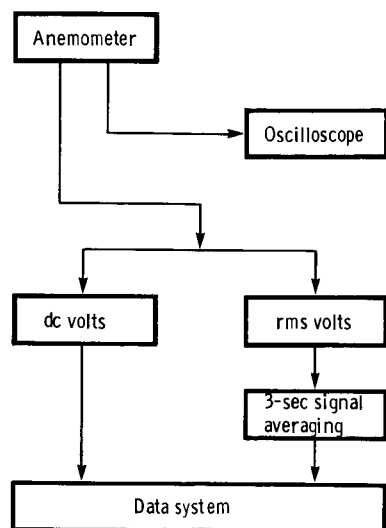
Figure 11.—Diagram of hot-wire circuit.

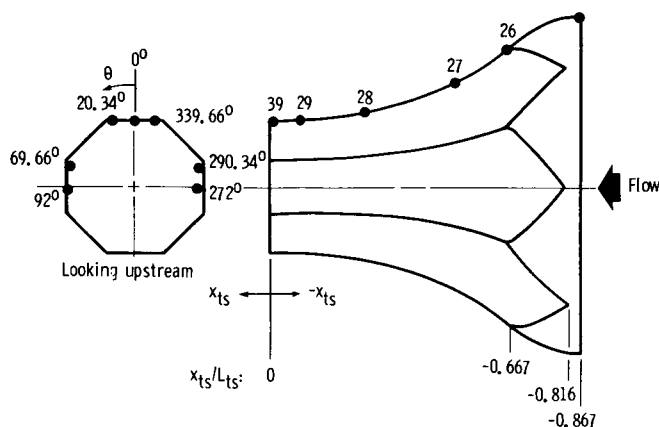| Static tap	Axial location,	Static tap	Axial location,
1	−0.851	21	−0.700
2	−.844	22	−.692
3	−.836	23	−.685
4	−.829	24	−.677
5	−.821	25	−.669
6	−.813	26	−.662
7	−.606	27	−.480
8	−.798	28	−.298
9	−.791	29	−.116
10	−.783	30	−.083
11	−.776	31	−.076
12	−.768	32	−.068
13	−.760	33	−.061
14	−.753	34	−.053
15	−.745	35	−.045
16	−.738	36	−.038
17	−.730	37	−.030
18	−.722	38	−.023
19	− 715	39	−.015
20	−.707		

Figure 12.—Wall static pressure taps in contraction section.

part of the contraction section, the static pressure taps were in the center of a flat and as close as possible to the corner of the same flat. The axial locations were chosen so that most of the static taps were in the two regions—one near the entrance and the other near the exit of the contraction section—where the potential for flow separation existed. All static taps were essentially square-edge orifices, 0.102 cm (0.040 in.) in diameter.

Screens and Honeycomb

The dimensions of the screens and the grid (a 1-mesh screen) chosen for evaluation are shown in table I. One major consideration was the screen open area, which should be greater than 57 percent (1) to prevent large nonuniformities in the velocity profile downstream of the screen caused by random coalescing of the jets emerging from the screen pores (ref. 14) and (2) to account for possible weaving errors resulting in local regions of small open area. However, the open area should not be much greater than 57 percent because the pressure drop would then be insufficient to substantially reduce the turbulence intensity. These considerations led to the choice of screens with an open area of 60 percent. A second major consideration was screen mesh. When multiple screens are used, the mesh should be fine enough for the turbulence from one screen to decay before the flow enters the next screen. But the mesh should not be so fine that dirt particles in the airstream clog the screen pores and thus reduce the open area. These considerations resulted in 34-mesh screens being chosen for multiple-screen configurations. Other considerations, to be mentioned later, were used in the selection of the 10-mesh screen and the 1-mesh grid.

All the screens as well as the grid were operated far above their critical Reynolds number of about 52 (table II) based on wire diameter and consequently had self-generated turbulence (ref. 15). For the screens this was small-scale turbulence that decayed rapidly with downstream distance so that far downstream the turbulence was below the original free-stream turbulence. Also, operating the screens far above their critical Reynolds number is advantageous because turbulence reduction is independent of the velocity approaching the screens (ref. 16).

TABLE I.—PHYSICAL PROPERTIES
OF SCREENS AND GRIDS

[Open area, 60 percent.]

Mesh	Wires per centimeter	Wires per inch	Wire diameter	
			cm	in.
1	0.39	1	0.572	0.225
10	3.94	10	.0572	.0225
34	13.39	34	.0168	.0066

TABLE II.—FLOW CONDITIONER REYNOLDS
NUMBERS BASED ON WIRE DIAMETER

Tunnel Mach number, M_{ts}	Settling chamber velocity, V_{sc}		Mesh		
			1	10	34
	m/sec	ft/sec	Reynolds number		
0.20	9.6	31.5	3 522	352	103
.40	19.2	63	7 133	713	209
.60	26.0	85.3	9 559	956	280
.80	29.0	95.1	10 957	1096	321
.916	30.5	100	11 237	1124	330

A honeycomb was also chosen for evaluation. Honeycombs are flow conditioners that suppress the level of incoming turbulence but in the process generate new turbulence (ref. 17). Suppression is due mostly to the reduction in the transverse components of the fluctuating velocity by the honeycomb side walls and is achieved in a very short distance downstream from the honeycomb entrance. Much of the new turbulence arises from shear layer instability occurring downstream of the honeycomb exit and increases with increasing honeycomb length. Consequently short honeycombs are attractive. Moreover, the shorter the honeycomb, the smaller the pressure loss. Honeycomb length should be no greater than 12 times the honeycomb cell size, according to reference 17. The honeycomb material was stainless steel. The honeycomb cell size was 0.953 cm (0.375 in.), its length was 11.4 cm (4.5 in.), and its open area was 98 percent. There is probably some optimum match between the scale of turbulence ahead of the honeycomb and the honeycomb cell size. However, as indicated in reference 18, tests to determine the effect of honeycomb cell size were inconclusive.

Nine honeycomb/screen configurations (fig. 13) were evaluated in the settling chamber. Configuration 1 had no honeycomb or screens and thus was the baseline used for comparison with all other configurations. Configuration 2 contained only the honeycomb located in the upstream part of the settling chamber. Configurations 3 to 6 contained the honeycomb followed by one to four 34-mesh screens, respectively. These four configurations represent the conventional method of simultaneously providing a uniform velocity profile and suppressing turbulence. For configurations 7 and 9 the honeycomb was located in the downstream part of the settling chamber with either a 34-mesh screen (configuration 7) or a 10-mesh screen (configuration 9) at the honeycomb exit. Screens used in this manner are referred to herein as exit plane screens. For configuration 8 the honeycomb was located in the upstream part of the settling chamber with a 10-mesh exit plane screen.

Some distance is required downstream of a screen or honeycomb for the turbulence to decay. For a screen this distance is 50 to 75 mesh lengths, or 330 to 500 wire diameters

(a) Configuration 1.   (f) Configuration 6.
(b) Configuration 2.   (g) Configuration 7.
(c) Configuration 3.   (h) Configuration 8.
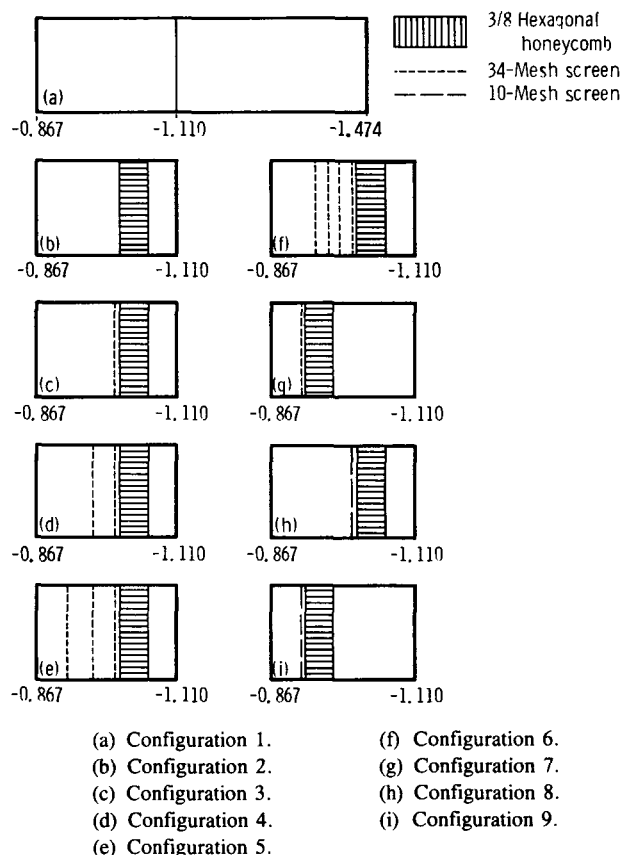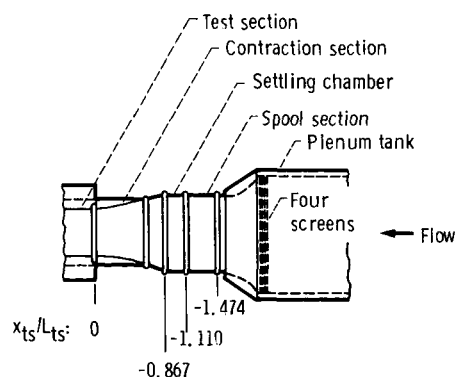(d) Configuration 4.   (i) Configuration 9.
(e) Configuration 5.

Figure 13.—Flow conditioner configurations tested in settling chamber.

(ref. 17). For a honeycomb the distance is about 50 cell diameters, or 1 to 10 cell lengths (ref. 17). When an exit plane screen is used with a honeycomb, the decay distance is independent of honeycomb cell diameter and length but is dependent on mesh ratio (i.e., the ratio of honeycomb mesh to screen mesh). For the mesh ratios used in the present investigation, 12.75 and 3.75, no information exists on decay distance. However, an indication of approximate decay distance can be obtained from reference 17, where a mesh ratio of 5.3 required a decay distance of 120 mesh lengths, or 800 wire diameters. If this criterion were applied to the present honeycomb/screen combinations, decay distance would be

TABLE III.—SCREEN SPACING CHARACTERISTICS

Flow conditioner configuration (fig. 13)	Spacing				Ratio of honeycomb mesh to screen mesh
	Between screens		Between grid and/or last screen and $x_{ts}/L_{ts} = -0.851$		
	Wire diameter	Mesh length	Wire diameter	Mesh length	
2	---	---	----	----	---
3	---	---	1163.64	261.12	12.75
4	303	68	860.61	193.12	
5	303	68	557.58	125.12	
6	303	68	254.55	57.12	
7	---	---	606.06	136.00	
8	---	---	341.33	76.80	
9	---	---	177.78	40.00	3.75

x_{ts}/L_{ts}: -1.474   -2.249   One 1-mesh grid
-1.962
(a)

x_{ts}/L_{ts}: -1.474   -2.011   -2.249   Four 34-mesh screens
-1.962
(b)

(a) One 1-mesh grid.
(b) Four 34-mesh screens.

Figure 14.—Flow conditioner configurations tested in plenum tank.

about 8.96 cm (120 mesh lengths divided by 13.39 meshes per centimeter) with the 34-mesh exit plane screen attached and about 30.46 cm (120 mesh lengths divided by 3.94 meshes per centimeter) with the 10-mesh screen attached. Decay distance for the honeycomb alone was about 47.65 cm (50 cell diameters multiplied by 0.953 cm per cell diameter). Thus decay distance for a honeycomb/screen combination will be greater than that for the screen alone but less than that for the honeycomb alone.

The spacing characteristics of the screens and the honeycomb chosen for the present test are presented in table III. For configurations where multiple screens were used (configurations 4 to 6), the allowable spacing between the second, third, and fourth screens (configurations 5 and 6) was questionable. Spacing was marginally adequate based on mesh length (68 mesh lengths as compared with a desired 50 to 75 mesh lengths) but inadequate based on wire diameter (303 wire diameters as compared with a desired 330 to 500 wire diameters). Spacing between the first and second screens was probably inadequate (see configuration 4). The first screen was located at the exit plane of the honeycomb and probably required something on the order of 120 mesh lengths rather than the 68 mesh lengths available between it and the second screen.

The hot-wire probes used to measure axial turbulence, as previously mentioned, were located at the contraction-section entrance. All configurations except 2, 7, 8, and 9 seemed to have sufficient distance downstream of the flow conditioner for almost all of the turbulence to decay before being measured by the hot-wire probes.

In addition to evaluating the honeycomb and the screens in the settling chamber, a limited study was done with some of them in the spool section. Since such configurations are not applicable to the full-scale AWT, they are discussed in an appendix.

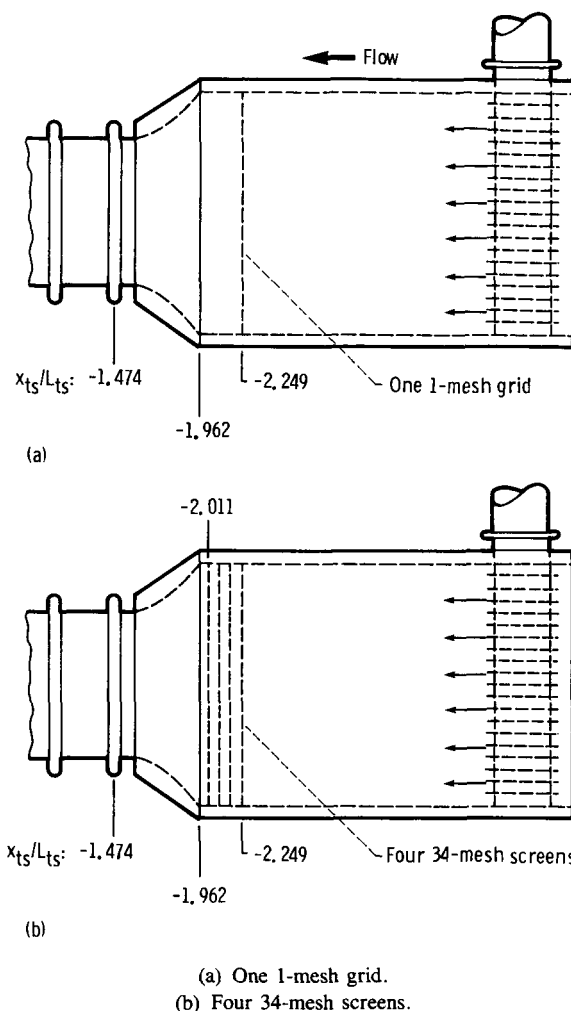Two screen configurations (fig. 14) located in the plenum tank also were investigated. The objectives of these studies were (1) to reduce both the nonuniformity and turbulence of the flow that entered the plenum tank through the supply pipe and (2) to achieve a turbulence level similar to that entering the settling chamber of the full-scale AWT, which was estimated to be about 6 percent. One configuration consisted of one 1-mesh grid, and the other consisted of four equally spaced (178-mesh-length spacing) 34-mesh screens. All had 60-percent open area and were located as far upstream as possible. The constraint on the farthest upstream location was that the plenum tank was designed to contain an acoustically treated torus that extended between the supply pipe and $x_{ts}/L_{ts} = -2.5$. The torus was not installed for these tests.

Procedure

For each test run data were taken at tunnel Mach numbers M_{ts} of 0.20, 0.40, 0.60, 0.80, and 0.916. The method for setting tunnel Mach number is given in reference 12. Test-section Reynolds number, based on the test-section equivalent diameter at the entrance, varied from 2.78×10^6 at $M_{ts} = 0.20$ to 9.16×10^6 at $M_{ts} = 0.916$.

(a) Tunnel Mach number, 0.20.   (d) Tunnel Mach number, 0.80.
(b) Tunnel Mach number, 0.40.   (e) Tunnel Mach number, 0.916.
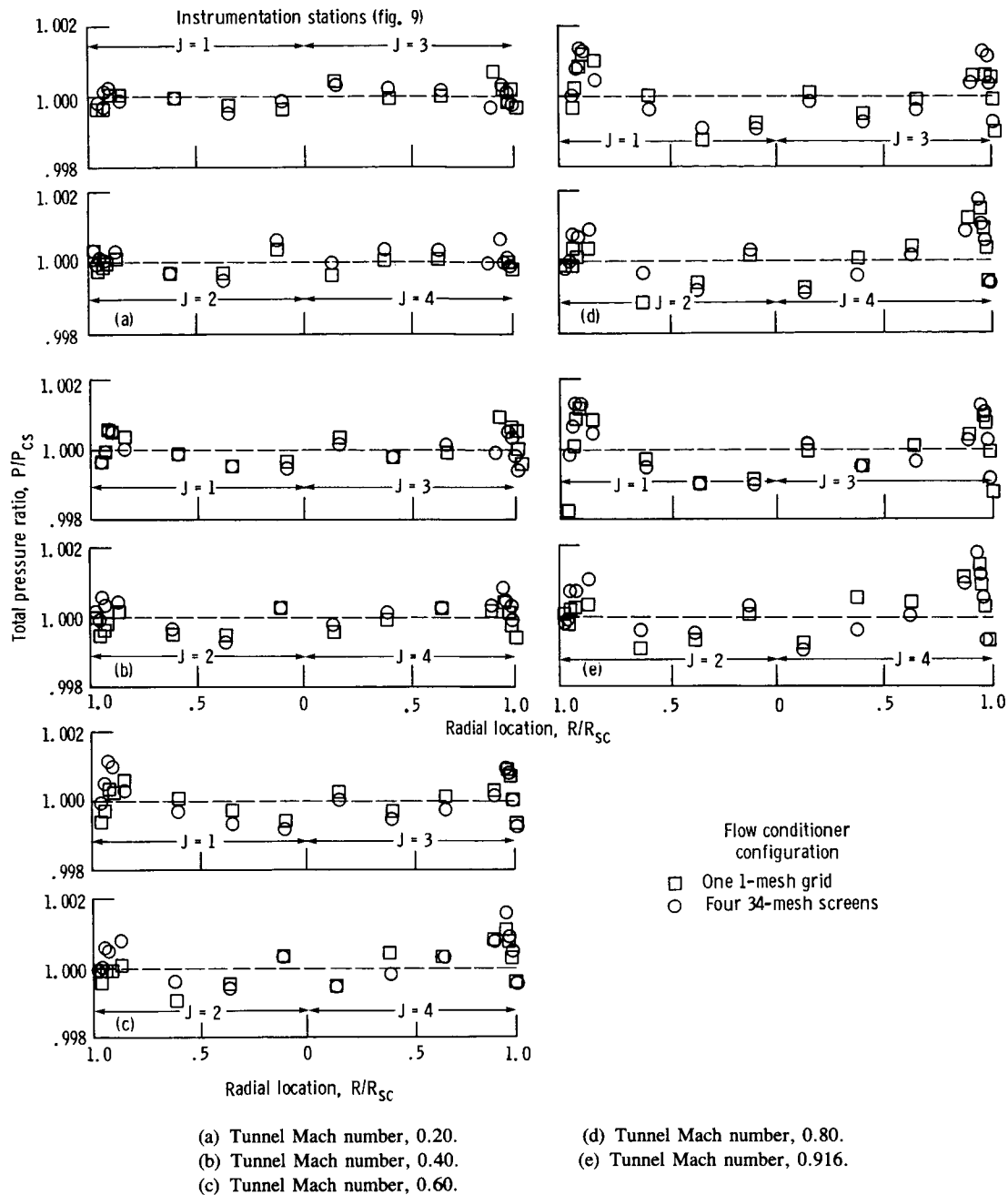(c) Tunnel Mach number, 0.60.

Figure 15.—Total pressure ratio profiles at contraction-section entrance for two screen configurations in plenum tank. Empty settling chamber and spool section.

Results and Discussion

Grid and Screens in Plenum Tank

Over the entire range of tunnel Mach numbers investigated there was no significant difference in total pressure ratio profile between the two screen configurations (fig. 15). Both the one 1-mesh grid and the four 34-mesh screens produced a small, nonuniform profile, which became more severe at M_{ts} of 0.60 and greater. The highest total pressure, about 0.1 percent above the average total pressure, occurred very close to the

wall of the settling chamber. The lowest total pressure, about 0.1 percent below the average total pressure, occurred near the center of the settling chamber. The profile probably was due to deflection of the grid and screens, as discussed later. With the four screens installed, longitudinal turbulence in the settling chamber was measured at 3.6 percent. No turbulence measurements were taken with the grid installed.

For the remaining tests the four 34-mesh screens were installed in the plenum tank. This configuration was selected (1) because the longitudinal value of turbulence was close to that estimated to enter the settling chamber of the full-scale
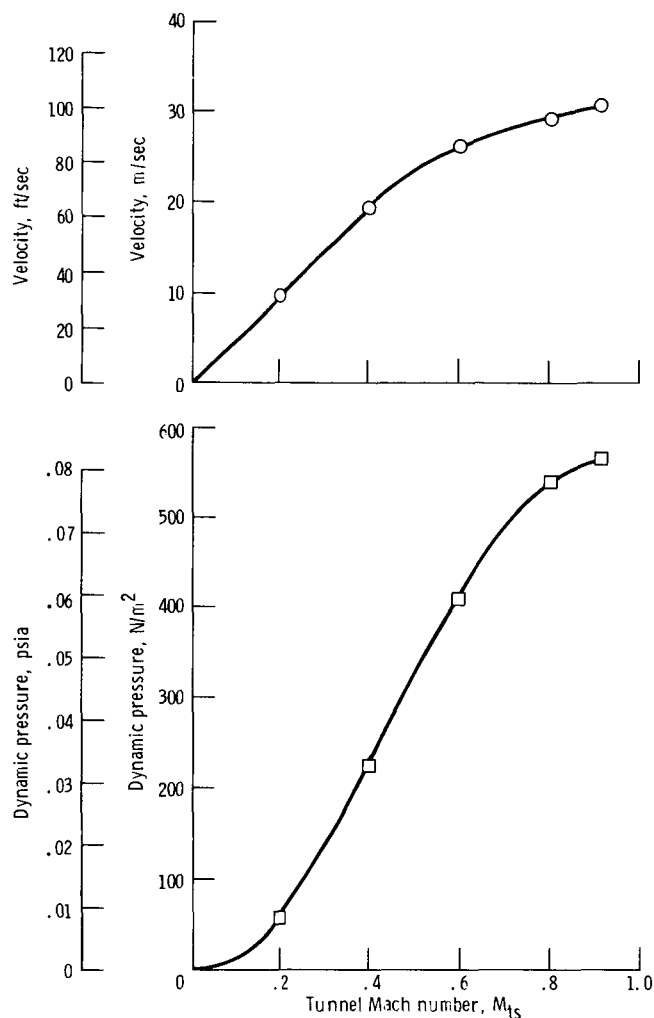
Figure 16.—Settling chamber velocity and dynamic pressure as function of tunnel Mach number.

TABLE IV.—EFFECT OF TUNNEL MACH NUMBER AND CIRCUMFERENTIAL LOCATION ON LONGITUDINAL TURBULENCE AT CONTRACTION-SECTION ENTRANCE

(a) Flow conditioner configuration 2 (fig. 13)

Tunnel Mach number, M_{ts}	Circumferential location, θ, deg			
	56¼	146¼	236¼	326¼
	Turbulence, percent			
0.20	2.5	2.7	2.7	2.5
.40	2.4	2.6	2.7	2.4
.60	2.5	2.6	2.6	2.4
.80	2.4	2.8	2.5	2.4
.916	2.5	2.8	2.4	2.3
Average	2.5	2.7	2.6	2.4

(b) Flow conditioner configuration 4 (fig. 13)

0.20	1.6	1.7	1.7	1.8
.40	1.4	1.4	1.6	1.6
.60	1.4	1.4	1.4	1.6
.80	1.4	1.5	1.4	1.6
.916	1.3	1.4	1.3	1.5
Average	1.4	1.5	1.5	1.6

(c) Flow conditioner configuration 6 (fig. 13)

0.20	1.6	1.6	1.5	1.6
.40	1.3	1.3	1.2	1.3
.60	1.2	1.2	1.2	1.2
.80	1.1	1.1	1.0	1.1
.916	1.1	1.1	1.0	1.0
Average	1.3	1.3	1.2	1.2

AWT and (2) because the option existed to increase the turbulence, if desired, by removing any of the four screens.

Screens and Honeycomb in Settling Chamber

With the two flow conditioner configurations installed in the settling chamber, the settling chamber velocity (fig. 16) varied from about 9.6 m/sec (31.5 ft/sec) at $M_{ts} = 0.20$ to about 30.5 m/sec (100 ft/sec) at $M_{ts} = 0.916$. Total pressure loss across each flow conditioner configuration is given in terms of a loss coefficient, defined as the total pressure loss divided by the dynamic pressure approaching the flow conditioner configuration. Settling chamber dynamic pressure (fig. 16) varied from 55 N/m^2 (0.008 psia) at $M_{ts} = 0.20$ to 565 N/m^2 (0.082 psia) at $M_{ts} = 0.916$.

Longitudinal turbulence measurements were taken at the contraction-section entrance over the entire range of tunnel Mach numbers at four circumferential locations. Results for three flow conditioner configurations (configurations 2, 4, and 6 as defined in fig. 13) are presented in table IV. They cover the range of longitudinal turbulence intensities from the highest to the lowest values measured. For each configuration turbulence intensity did not vary significantly with either tunnel Mach number or circumferential location. This trend is typical of the turbulence intensity measured downstream of all the flow conditioner configurations and, as already mentioned, was due to the screens being operated far above their critical Reynolds number. Consequently turbulence intensity results presented in the remainder of this report for each flow conditioner configuration are the average value obtained over the entire Mach number range at all four circumferential locations.

In an attempt to estimate the accuracy of the hot-wire measurements the data presented in table IV were evaluated by using small-sample statistical theory. The arithmetic mean value of longitudinal turbulence was determined along with the 95-percent confidence limits for the true mean value and

TABLE V.—ESTIMATED HOT-WIRE MEASUREMENT ACCURACY

Flow conditioner configuration (fig. 13)	Mean value of turbulence, percent	95-Percent confidence limit, percent	Measurement accuracy, percent
2	2.54	2.47–2.60	±2.8
4	1.50	1.43–1.57	±4.7
6	1.24	1.14–1.33	±8.1

the resulting accuracy. The results are presented in table V. For the 20 measurements associated with configuration 2, which resulted in an arithmetic mean turbulence of 2.54 percent, there is 95-percent confidence that the true mean value of turbulence lies somewhere between 2.47 and 2.60 percent. This results in a hot-wire measurement accuracy of about ±2.8 percent. Hot-wire measurement accuracy decreases with decreasing turbulence. For configuration 4, which had an arithmetic mean turbulence of 1.5 percent, measurement accuracy was about ±4.7 percent; for configuration 6, which had the second lowest arithmetic mean turbulence, 1.24 percent, measurement accuracy was about ±8 percent. Thus the accuracy of measuring longitudinal turbulence for all configurations was a function of turbulence value and was assumed to vary from ±2.5 percent for the highest value of turbulence to ±8 percent for the lowest value of turbulence.

Conventional configurations.—The first set of flow conditioner configurations evaluated (configurations 2 to 6 in fig. 13) represented the conventional type generally installed in wind tunnels. A honeycomb was installed in the upstream part of the settling chamber to reduce lateral turbulence and was followed by a series of screens to simultaneously provide a uniform velocity profile and a reduction in turbulence. Turbulence in the empty settling chamber was 3.6 percent (fig. 17). Installing the honeycomb reduced the turbulence to 2.6 percent. Although a honeycomb is not generally noted for reducing the longitudinal component of turbulence, similar reductions in longitudinal turbulence are reported in reference 19. A honeycomb followed by three 34-mesh screens reduced the turbulence to 1.2 percent. Adding a fourth 34-mesh screen did not further reduce turbulence. Some, as yet unknown, disturbance was probably forming a "floor." More will be said about this later.

The total pressure loss coefficient decreased sharply with increasing tunnel Mach number up to about $M_{ts} = 0.40$ and then remained essentially constant with further increases in Mach number (fig. 18). For a given tunnel Mach number the loss coefficient was lowest when only the honeycomb was installed and highest when the honeycomb plus four screens were installed. At $M_{ts} = 0.80$ the total pressure loss across the honeycomb alone was about half the dynamic pressure in the settling chamber, and the total pressure loss across the honeycomb plus four screens was about three times the dynamic pressure.
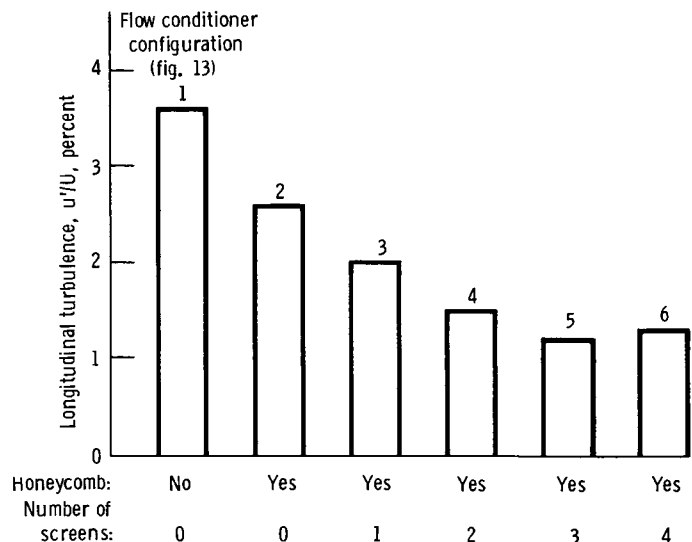

Figure 17.—Effect on longitudinal turbulence at contraction-section entrance of honeycomb alone and in combination with up to four fine-mesh screens.
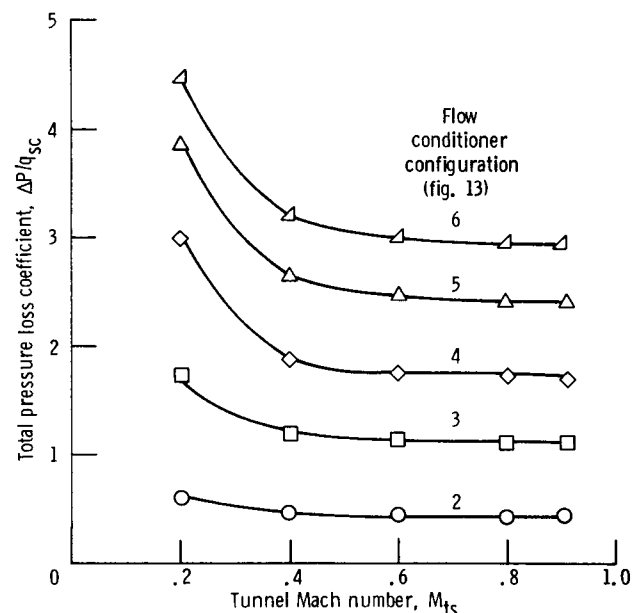

Figure 18.—Total pressure loss coefficient across honeycomb alone and in combination with up to four fine-mesh screens.

The total pressure loss across the honeycomb plus four screens (configuration 6) was substantially greater than that across the honeycomb plus three screens (configuration 5). Consequently a reduction in turbulence was expected when the fourth screen was added. But, as shown in figure 17, the hot-wire sensor did not measure a reduction. However, the hot-wire sensor system does not separate acoustical waves from vorticity (fluid turbulence). Honeycombs and screens primarily modify fluid turbulence but have little effect on acoustical waves. This suggests that the disturbance forming the floor, discussed in connection with figure 17, could be acoustical. But, as the following discussion suggests, it might also be due to inadequate spacing between screens.
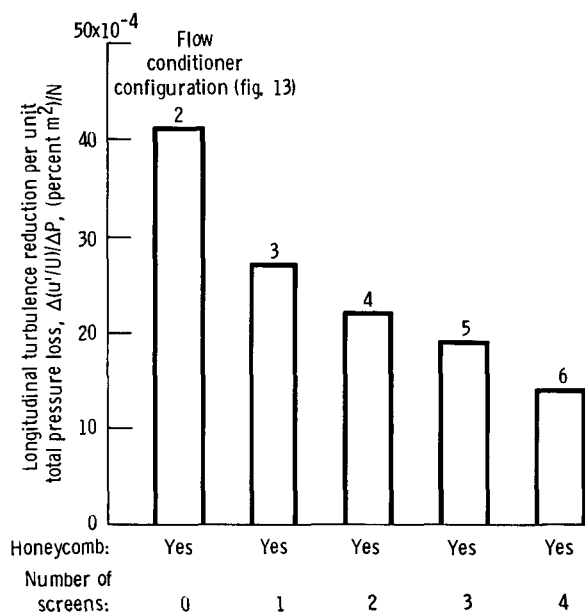
13

Figure 19.—Effectiveness at contraction-section entrance of honeycomb alone and in combination with up to four fine-mesh screens. Tunnel Mach number, 0.80.

Effectiveness is expressed as the reduction in longitudinal turbulence divided by the total pressure loss across the configuration. The larger the value, the more turbulence reduction for a given total pressure loss and consequently the more effective the configuration. The honeycomb-alone configuration was the most effective (fig. 19), with a value of 41×10^{-4} (percent m^2)/N. Adding screens reduced the effectiveness; the more screens, the lower the effectiveness. This suggested that the spacing between the screens was inadequate for the turbulence to decay before entering the next screen. As mentioned in the section Apparatus and Procedure, the spacing between screens was questionable. Thus the floor might be due to inadequate spacing between screens. Time limitations precluded an investigation to establish the exact cause of the floor.

As previously mentioned, a small nonuniform total pressure profile existed in the empty settling chamber, with the highest total pressure very close to the wall and the lowest total pressure near the center of the chamber. Installing the honeycomb alone or in combination with an exit plane screen in the upstream part of the settling chamber did not significantly affect the total pressure profile over the entire range of tunnel Mach numbers tested (fig. 20). Adding the remaining three screens, however, did have an adverse effect for M_{ts} of 0.40 and higher. The principal effect was to lower the total pressure near the center of the settling chamber, resulting in a steeper total pressure gradient between the wall and the center of the chamber. This occurred when the number of screens remained constant and the tunnel Mach number increased as well as when the tunnel Mach number was held constant and the number of screens increased. For example, at $M_{ts} = 0.80$, increasing the number of screens from one to four lowered the total pressure from about 0.15 percent to about 0.30 percent below the average total pressure. Keeping the number of screens constant at four and increasing the tunnel Mach number from 0.40 to 0.916 lowered the total pressure from about 0.15 percent to about 0.35 percent below the average total pressure. The increase in the total pressure gradient with increasing tunnel Mach number also suggests bending of the screens; bending would increase with increasing Mach number (i.e., increasing dynamic pressure).

Note that the overall shape of the total pressure ratio profile shown in figure 20 was the same regardless of how many screens were added. That is, the highest total pressure occurred very close to the wall and was followed by a rapid decrease in pressure with the lowest total pressure occurring near the center of the settling chamber. This is the type of profile produced when a screen bends; and the more the bend, the worse the profile (ref. 20). Thus a possible explanation for this profile is that the screens were bending.

Honeycomb/screen axial locations and mesh ratios. —The configurations discussed so far (configurations 2 to 6) represented the conventional approach for simultaneously providing a uniform velocity profile and suppressing turbulence. The remaining discussion in this section will be concerned with configurations to determine (1) the effects of honeycomb/screen axial location and (2) the effects of honeycomb/screen mesh ratio.
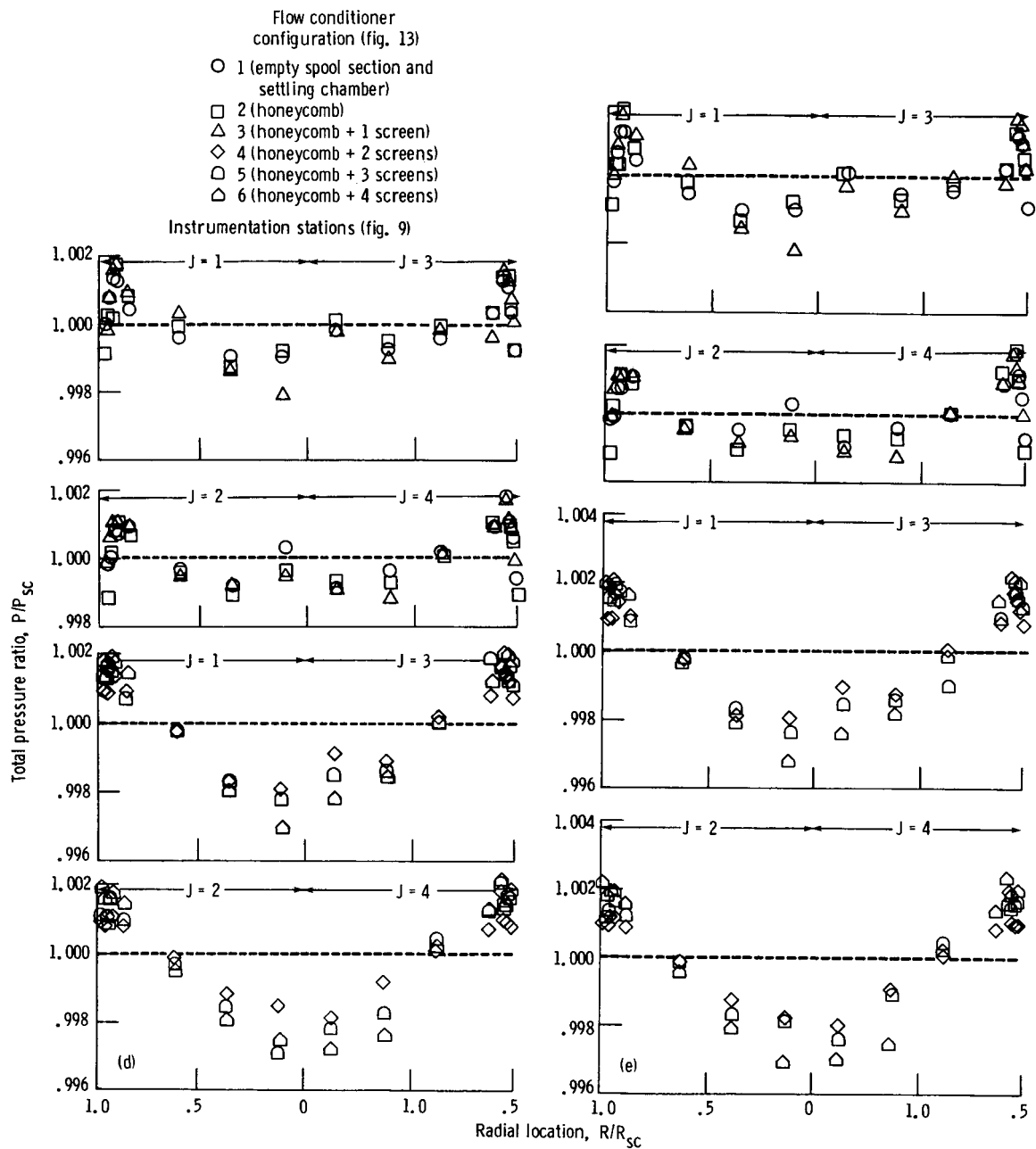
The purposes of the exit plane screen, as already mentioned, were (1) to chop up the honeycomb-generated turbulence into smaller-scale, faster-dissipating turbulence and (2) to reduce the turbulence exiting from the honeycomb. Moving the honeycomb/screen configurations from their upstream location to their downstream location at the contraction-section entrance had an adverse effect on turbulence. For the 34-mesh exit plane screen (fig. 21(a)) turbulence increased from 2 to 2.6 percent; for the 10-mesh exit plane screen (fig. 21(b)) turbulence increased from 1.8 to 2.2 percent. Note that lower turbulence values were measured with the 10-mesh exit plane screen for both the upstream and downstream locations of the honeycomb/screen combination. This suggests that the adverse effect was not due to the screen. If the screen alone were at the downstream location, the measured turbulence would have been higher with the 10-mesh screen than with the 34-mesh screen. The adverse effect was probably due to the mesh ratio between honeycomb and screen not being optimum and thus requiring a greater distance for the honeycomb-generated turbulence to decay. The lower turbulence values with the 10-mesh screen suggest that a mesh ratio of 3.75 is closer to the optimum than 12.75.

As expected, the total pressure loss coefficient was independent of honeycomb/screen axial location for configurations 3, 7, 8, and 9 (fig. 22). Also, for M_{ts} of 0.60 and greater total pressure loss coefficient was independent of whether a 10-mesh or a 34-mesh exit plane screen was used. Thus total pressure loss coefficient was independent of
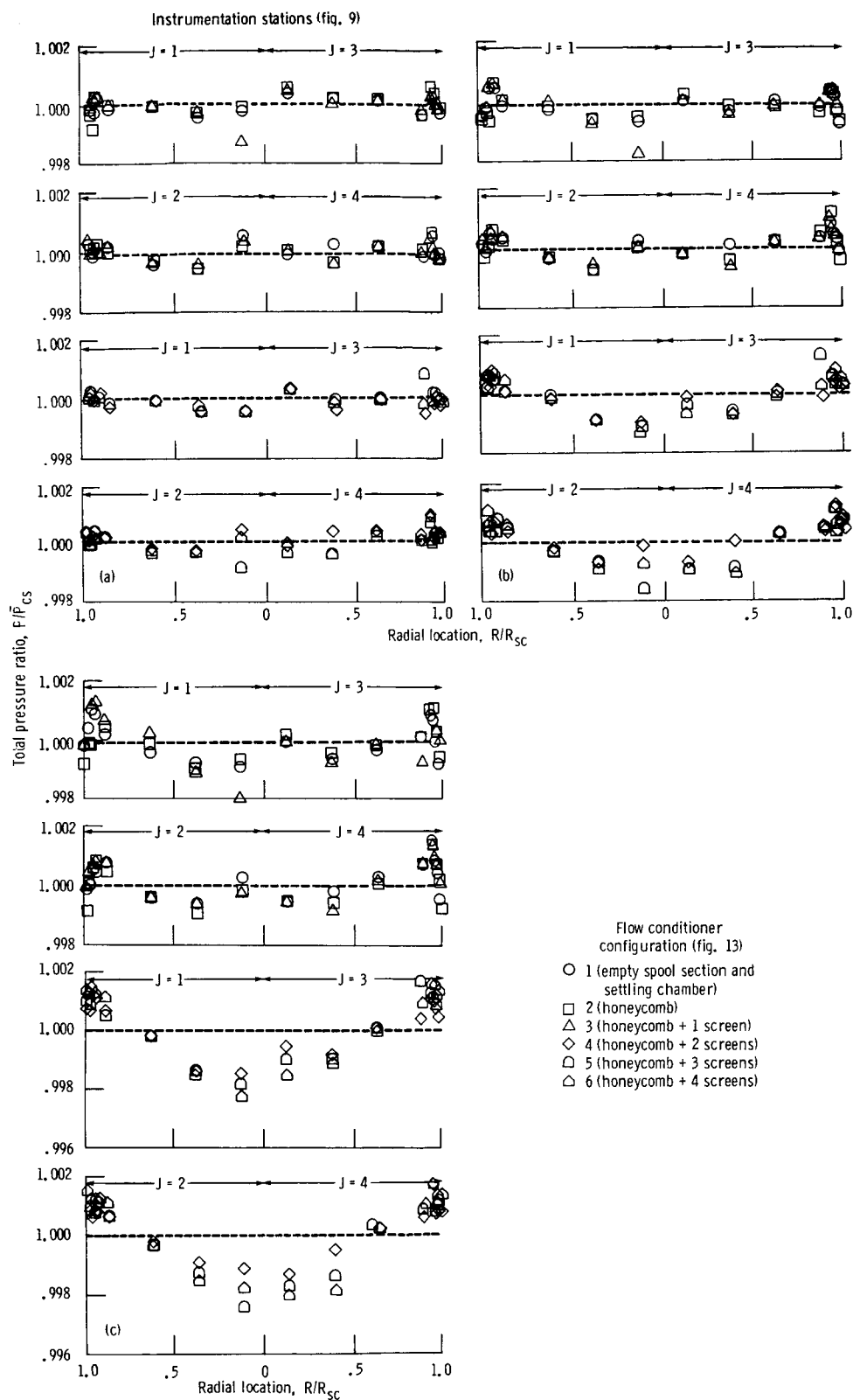
(a) Tunnel Mach number, 0.20.
(b) Tunnel Mach number, 0.40.
(c) Tunnel Mach number, 0.60.

Figure 20.—Effect on total pressure ratio profile at contraction-section entrance of honeycomb alone and in combination with fine-mesh screens.
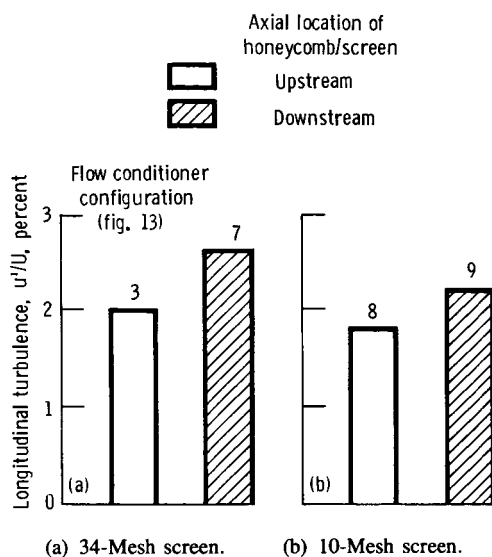
15

Flow conditioner
configuration (fig. 13)

○ 1 (empty spool section and
    settling chamber)
□ 2 (honeycomb)
△ 3 (honeycomb + 1 screen)
◇ 4 (honeycomb + 2 screens)
⌂ 5 (honeycomb + 3 screens)
△ 6 (honeycomb + 4 screens)

Instrumentation stations (fig. 9)

(d) Tunnel Mach number, 0.80.
(e) Tunnel Mach number, 0.916.

Figure 20.—Concluded.

Flow conditioner
configuration
(fig. 13)

(a) 34-Mesh screen. (b) 10-Mesh screen.

Figure 21.—Effect on longitudinal turbulence at contraction-section entrance of axial location of honeycomb screen.

Flow conditioner
configuration
(fig. 13)

○ 3
▢ 7

◇ 8
△ 9

Tunnel Mach number, M_{ts}

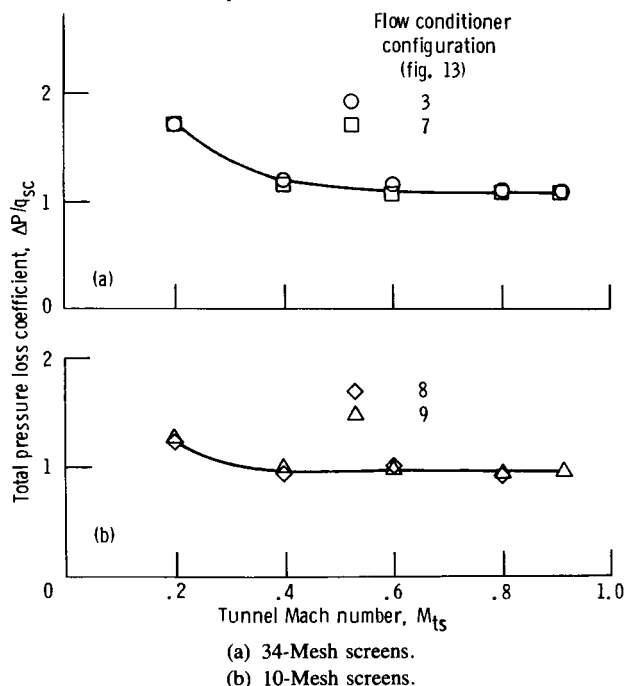(a) 34-Mesh screens.
(b) 10-Mesh screens.

Figure 22.—Effect of axial location on total pressure loss coefficient across honeycomb screen.

honeycomb/screen mesh ratio for M_{ts} of 0.60 and greater. At $M_{ts} = 0.80$ total pressure loss across the honeycomb/screen combination was equal to the dynamic pressure in the settling chamber.

At either axial location the honeycomb was more effective with the 10-mesh screen than with the 34-mesh screen (fig. 23). This was due entirely to the greater reduction in turbulence with the 10-mesh screen since, as just mentioned, total pressure loss was independent of mesh ratio and axial location.

Moving the honeycomb/screen configurations from their upstream location to their downstream location (contraction-

Axial location of
honeycomb/screen

▢ Upstream

▨ Downstream

40×10^{-4}

Flow conditioner
configuration
(fig. 13)

3
7
8
9

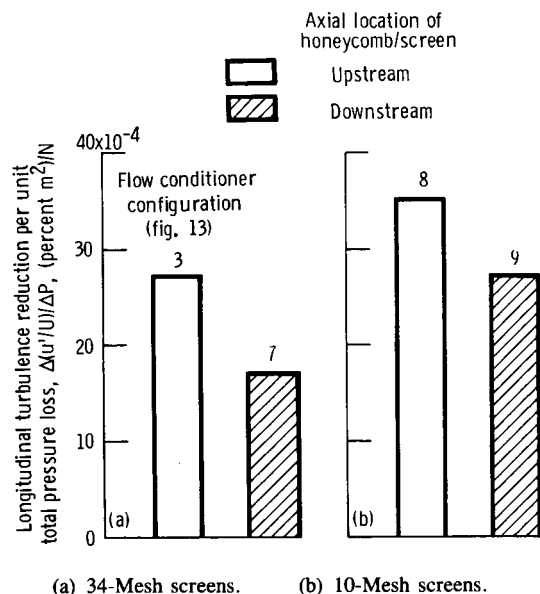(a) 34-Mesh screens. (b) 10-Mesh screens.

Figure 23.—Effectiveness at contraction-section entrance of axial location of honeycomb screen.

section entrance) in the settling chamber increased the adverse effect on total pressure ratio profile for M_{ts} of 0.60 and greater (fig. 24). The principal effect was to reduce the total pressure near the center of the settling chamber. The adverse effect was not significantly different with the 34-mesh exit plane screen from that with the 10-mesh exit plane screen. At $M_{ts} = 0.80$ the total pressure was about 0.20 percent below the average total pressure for both exit plane screens. The adverse effect was attributed to bending of the screens, which, as previously mentioned, would result in the type of total pressure profile shown. Although the 34-mesh screen had considerably smaller diameter wires than the 10-mesh screen (0.0168 cm (0.0066 in.) vs. 0.0572 cm (0.0225 in.)), this did not significantly affect the total pressure ratio profile. Apparently much larger diameter wires are required to alleviate the bending problem. A wire diameter of 0.572 cm (0.225 in.), as shown in the appendix, seemed to be sufficiently large.

As mentioned, the adverse effect on total pressure ratio profile was less when the honeycomb/screen configurations were located in the upstream part of the settling chamber. The reason was probably that more length was available for flow mixing, resulting in a more uniform profile.

Contraction-Section Wall Mach Number Distribution

The contraction section is quite short, $L_{cs}/D_{max,cs} = 0.935$, for the amount of area ratio reduction, $A_{max,cs}/A_{ts} = 6.305$. Some contraction sections this short have exhibited flow separation problems (ref. 21). The potential for flow separation exists in two regions: one near the entrance and the other near the exit of the section. Because contractions considerably reduce boundary layer thickness, however, separation near the entrance usually will be the dominant factor. Analytical analysis of the present contraction section (ref. 4) indicates
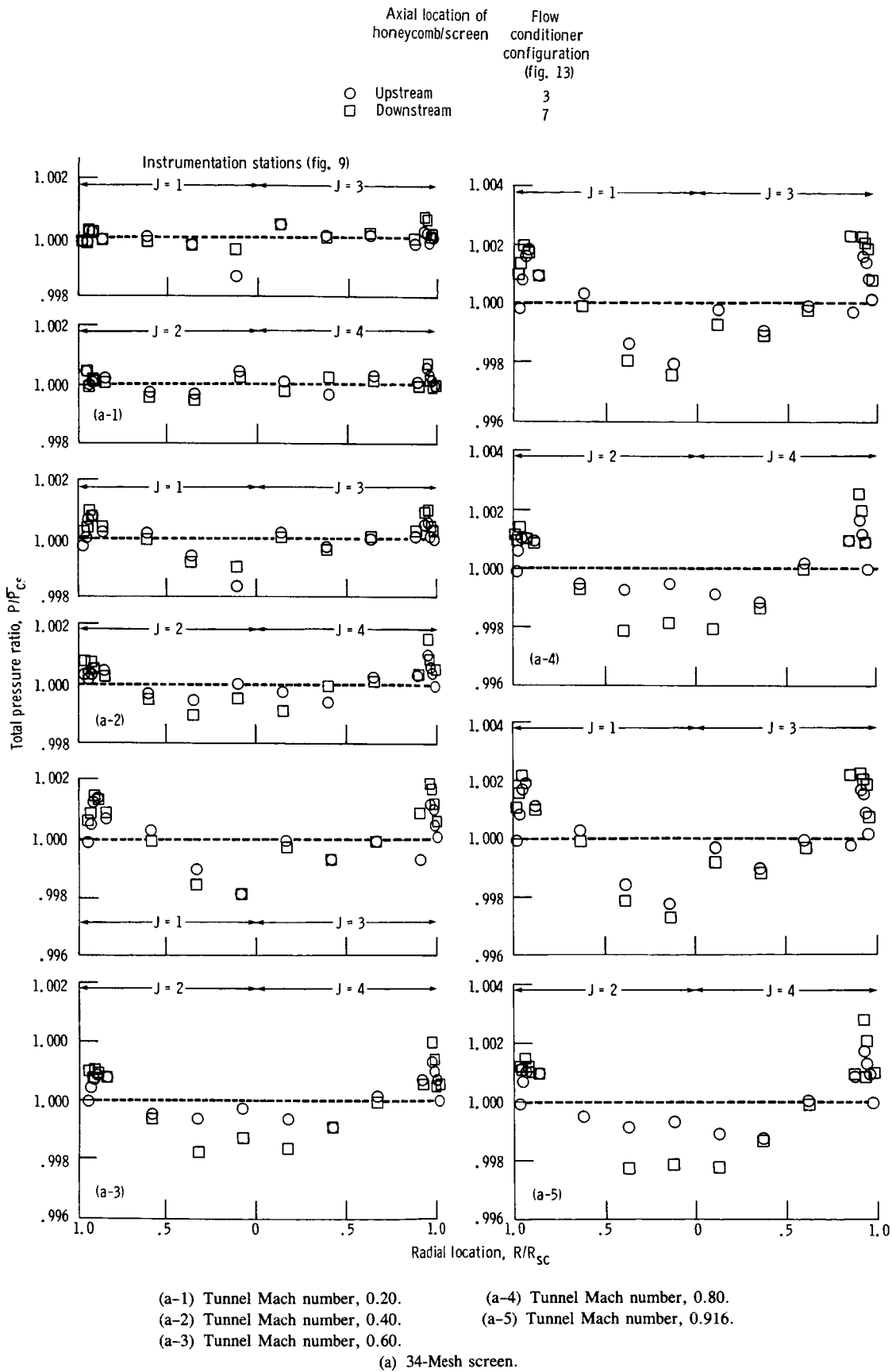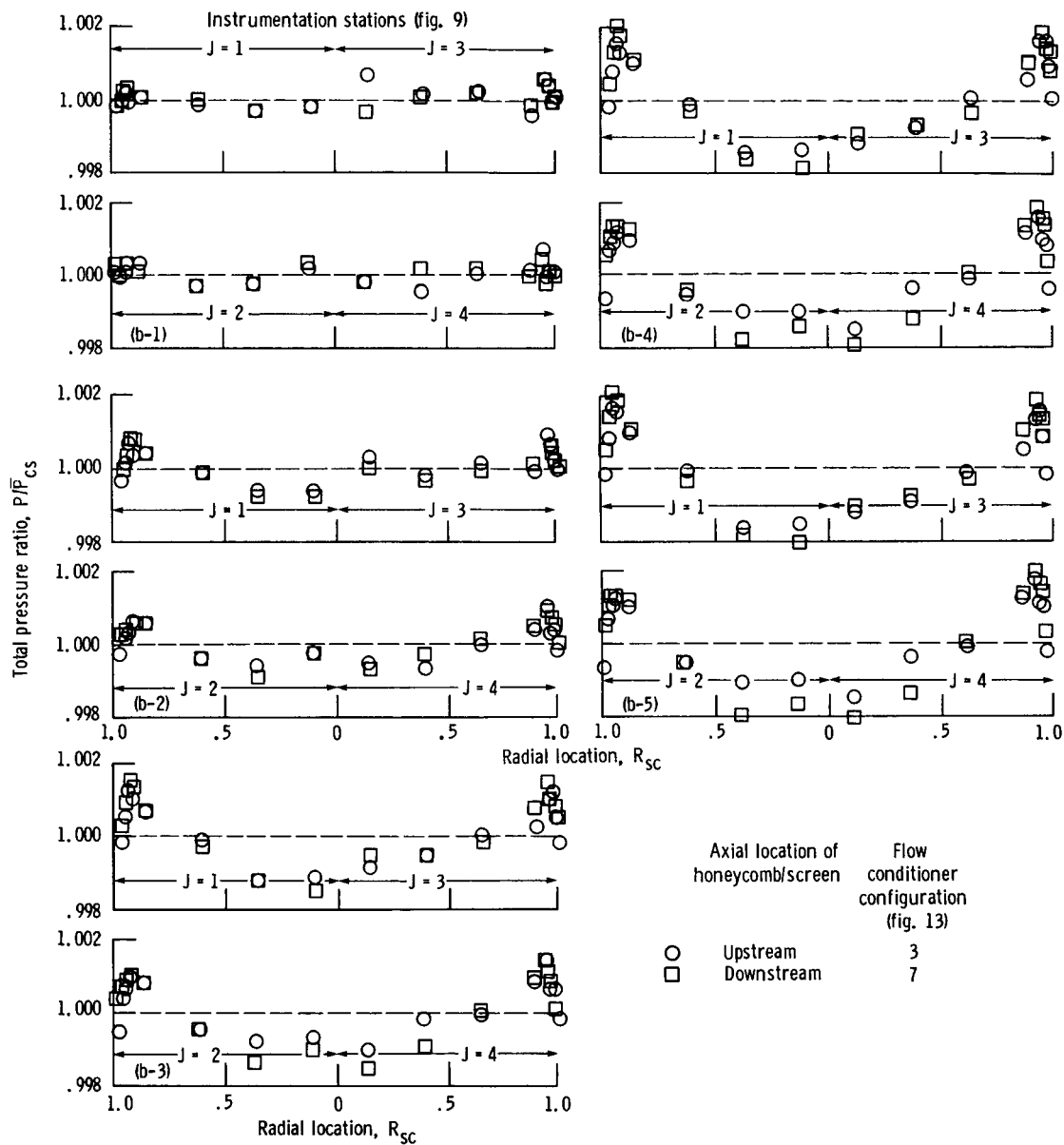
Figure 24.—Effect on total pressure ratio profile at contraction-section entrance of axial location of honeycomb screen.

(a-1) Tunnel Mach number, 0.20.   (a-4) Tunnel Mach number, 0.80.
(a-2) Tunnel Mach number, 0.40.   (a-5) Tunnel Mach number, 0.916.
(a-3) Tunnel Mach number, 0.60.

(a) 34-Mesh screen.

(b–1) Tunnel Mach number, 0.20.   (b–4) Tunnel Mach number, 0.80.
(b–2) Tunnel Mach number, 0.40.   (b–5) Tunnel Mach number, 0.916.
(b–3) Tunnel Mach number, 0.60.

(b) 10-Mesh screen.

Figure 24.—Concluded.

19

the possibility of flow separation near the entrance. Separation could lead to lower flow quality in the test section.

Static pressure measurements were made at seven circumferential locations along the length of the contraction section. The resulting surface Mach numbers at circumferential locations of 0° (center of the top octagonal flat), 20.34° (near one corner of that flat) and 339.66° (near the other corner of that flat) are shown in figure 25. No flow conditioner configurations were installed in the settling chamber. The well-behaved shape of the surface Mach number distribution indicates attached flow along the entire length of the contraction section. Results at the other four circumferential locations were similar and therefore are not presented herein. Observation of tufts located on other flats at the center and near the corners also did not show any signs of flow separation over the entire tunnel Mach number range.

Expanding both the abscissa and the ordinate scales allowed a closer examination of the wall Mach number distribution in the upstream part of the contraction section from x_{ts}/L_{ts} of -0.867 to -0.667 (fig. 26). The flow remained attached because only a very small adverse pressure gradient occurred near the contraction-section entrance. The flow also accelerated slightly faster along the center of the flats than near the corners. This was caused by the higher wall curvature of the flats in contrast to the corners as the cross section transitioned from circular at $x_{ts}/L_{ts} = -0.816$ to octagonal at $x_{ts}/L_{ts} = -0.667$.

Flow near the contraction-section entrance may be influenced by the axial location of the honeycomb/screen configuration in the settling chamber. According to reference 4, the closer the honeycomb/screen is to the contraction-section entrance, the less likely the flow is to separate.

The wall Mach number distribution was recorded in the upstream part of the contraction section at 0° circumferential location (fig. 27) for the honeycomb/screen in its farthest upstream location and in its farthest downstream location (fig. 28). A 34-mesh exit plane screen was used with each configuration. Locating the honeycomb/screen in the farthest upstream location had no significant effect on the wall Mach number in the upstream part of the contraction section. Thus it did not affect the adverse gradient. Locating the honeycomb/screen in its farthest downstream location decreased the wall Mach number distribution slightly between x_{ts}/L_{ts} of -0.867 and -0.700. It was most noticeable at M_{ts} of 0.60 and above and might be a small region of separated flow caused by misalignment between the screen and the contraction-section entrance, resulting in a small rearward-facing step. At $x_{ts}/L_{ts} = -0.770$ the flow had reattached and started to accelerate, achieving the same value as in the empty settling chamber at $x_{ts}/L_{ts} = -0.667$. Thus the wall Mach number distribution in the upstream part of the contraction section was not significantly affected by the axial location of the honeycomb/screen in the settling chamber.
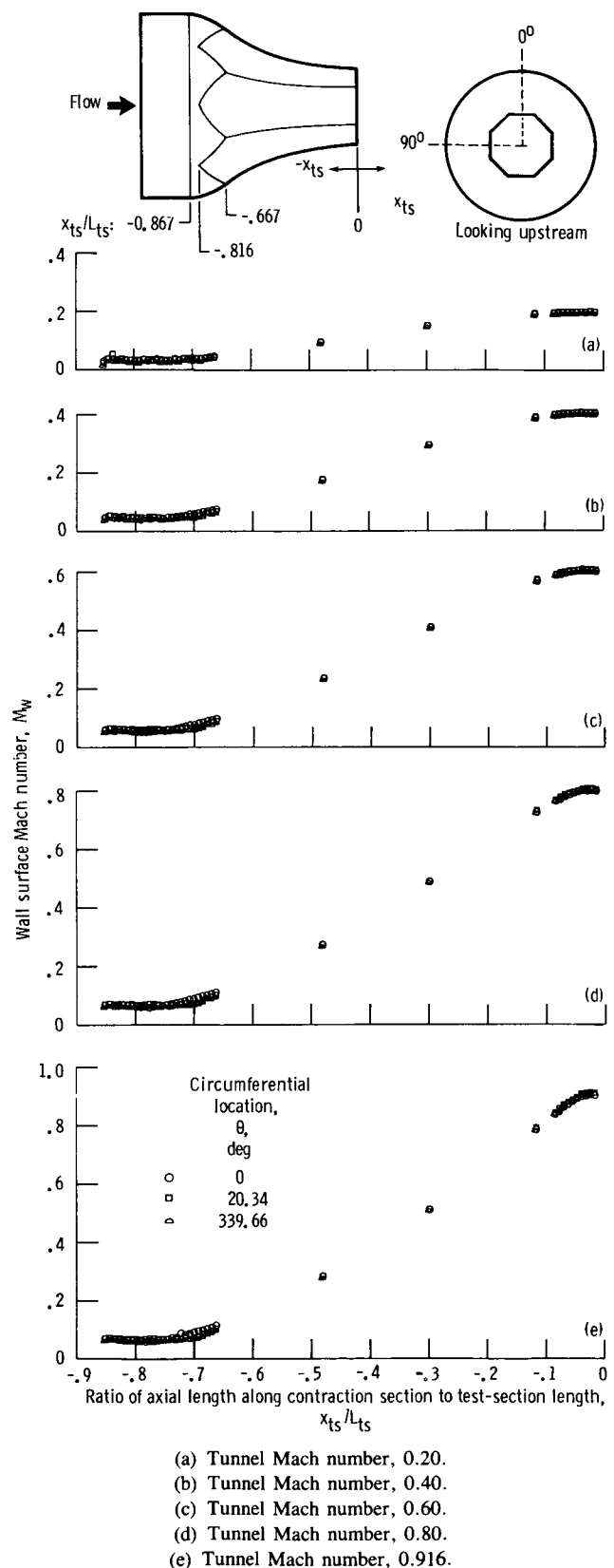

(a) Tunnel Mach number, 0.20.
(b) Tunnel Mach number, 0.40.
(c) Tunnel Mach number, 0.60.
(d) Tunnel Mach number, 0.80.
(e) Tunnel Mach number, 0.916.

Figure 25.—Wall Mach number distribution along entire contraction section at three circumferential locations. Empty settling chamber.

(a) Tunnel Mach number, 0.20.
(b) Tunnel Mach number, 0.40.
(c) Tunnel Mach number, 0.60.
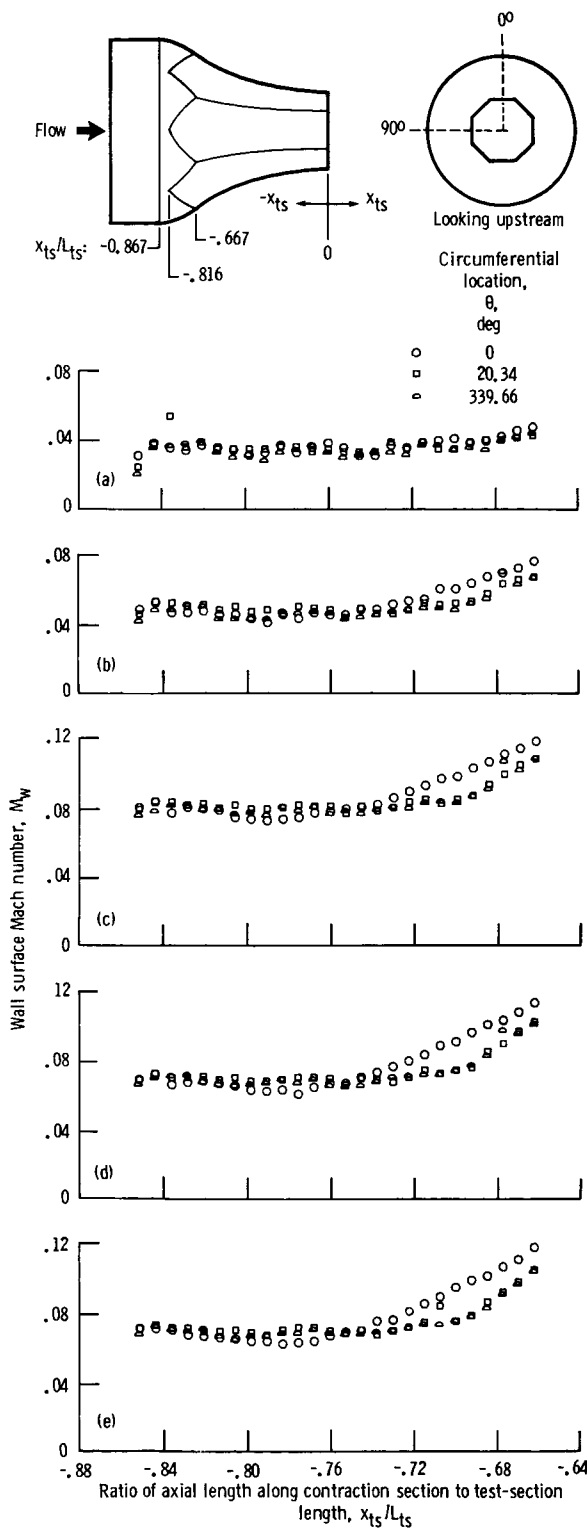(d) Tunnel Mach number, 0.80.
(e) Tunnel Mach number, 0.916.

Figure 26.—Wall Mach number distribution along upstream part of contraction section at three circumferential locations. Empty settling chamber.

(a) Tunnel Mach number, 0.20.
(b) Tunnel Mach number, 0.40.
(c) Tunnel Mach number, 0.60.
(d) Tunnel Mach number, 0.80.
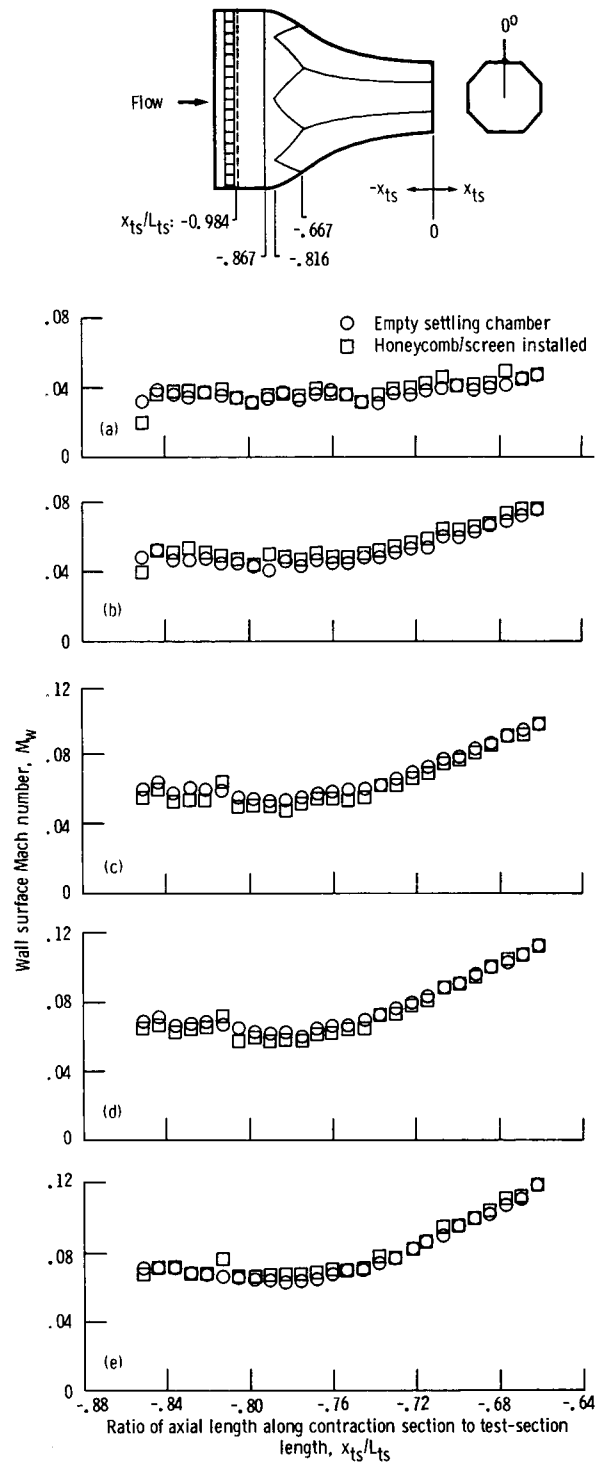(e) Tunnel Mach number, 0.916.

Figure 27.—Effect of honeycomb/screen configuration near settling chamber inlet on wall Mach number distribution along upstream part of contraction section.
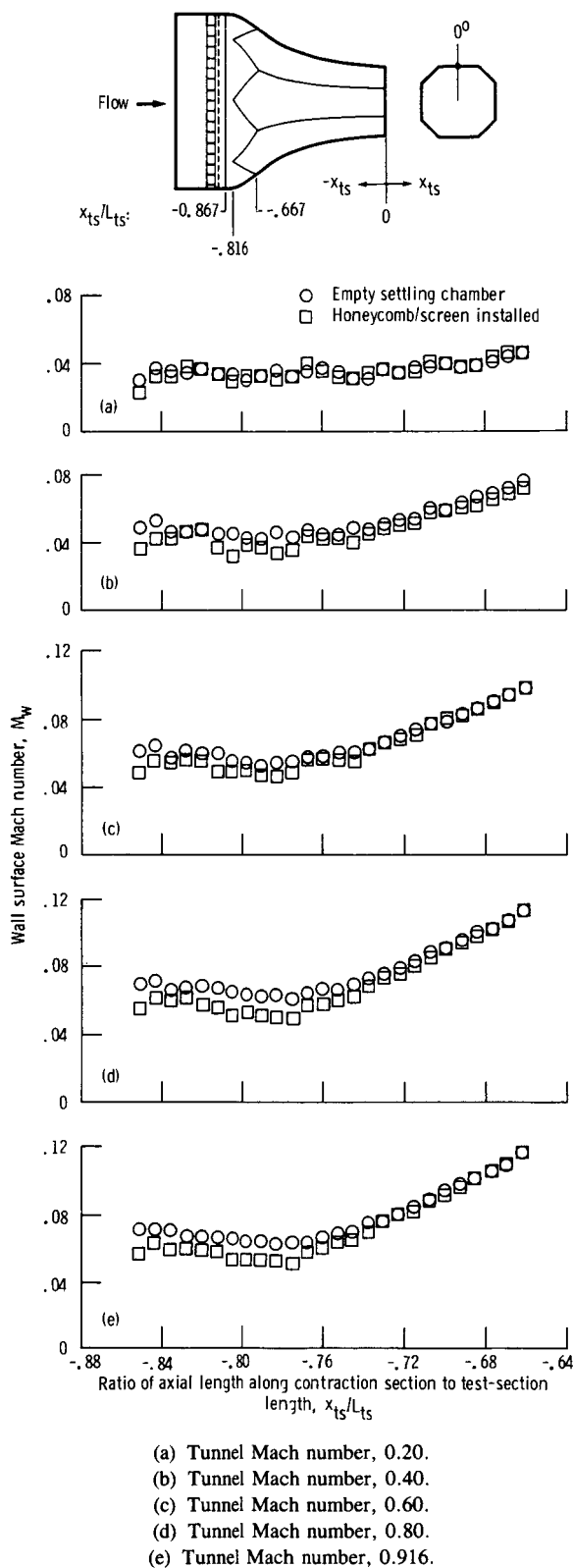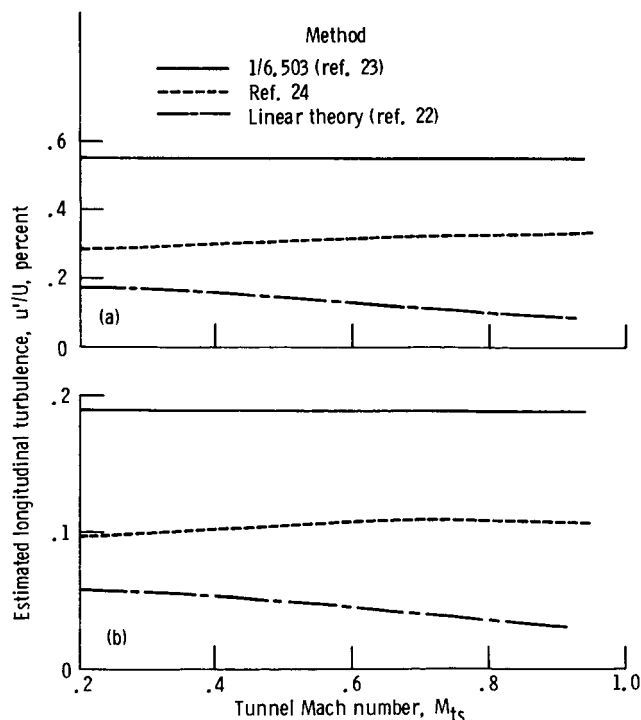
Estimated Longitudinal Turbulence in Test Section

As already mentioned, the highest value of longitudinal turbulence, 3.6 percent, was measured in the settling chamber when it was empty (i.e., no flow conditioners installed); the lowest value, 1.2 percent, was measured with the honeycomb plus three screens installed in the settling chamber. Longitudinal turbulence in the test section was estimated for the highest and lowest values of turbulence measured in the settling chamber (fig. 29). The estimates were based on three methods of determining the turbulence reduction through contraction sections. Of the three, the linear theory of reference 22 predicted the greatest reduction in turbulence. Longitudinal turbulence in the test section, at $M_{ts} = 0.80$, was estimated to be 0.10 percent for the highest and 0.035 percent for the lowest values of turbulence in the settling chamber. The second estimate, which predicted the smallest reduction in longitudinal turbulence, was based on an assessment of several NASA wind tunnels (ref. 23). Longitudinal turbulence in the test section, at $M_{ts} = 0.80$, was estimated to be 0.55 percent for the highest and 0.19 percent for the lowest value of turbulence in the settling chamber. The third estimate, which falls between the two just mentioned, was based on the empirical results of reference 24. Longitudinal turbulence in the test section, at $M_{ts} = 0.80$, was estimated to be 0.32 percent for the highest and 0.11 percent for the lowest value of turbulence in the settling

(a) Tunnel Mach number, 0.20.
(b) Tunnel Mach number, 0.40.
(c) Tunnel Mach number, 0.60.
(d) Tunnel Mach number, 0.80.
(e) Tunnel Mach number, 0.916.

Figure 28.—Effect of honeycomb/screen configuration near settling chamber exit on wall Mach number distribution along upstream part of contraction section.

(a) 3.6-Percent longitudinal turbulence in empty settling chamber.
(b) 1.20-Percent longitudinal turbulence with honeycomb plus three screens in settling chamber.

Figure 29.—Estimated longitudinal turbulence in test section for highest and lowest turbulence values measured in settling chamber.

chamber. Thus for an empty settling chamber the estimated longitudinal turbulence in the test section varied between 0.10 and 0.55 percent. With the honeycomb plus three screens installed in the settling chamber, the three values of estimated longitudinal turbulence in the test section were 0.035, 0.10, and 0.19 percent.

The turbulence intensity goal for the 0.1-scale model of the AWT test section was 0.50 percent (ref. 7). This value included the two transverse components as well as the longitudinal component of turbulence. Contraction sections do not reduce the transverse components as much as the longitudinal component. Therefore the turbulence intensity (including all three components) in the test section will be greater than 0.035 percent and probably will be between 0.10 and 0.20 percent. Thus the goal of 0.50 percent turbulence in the test section should easily be surpassed.

Summary of Results

An experimental investigation was conducted in the high-speed leg of the 0.1-scale model of the proposed Altitude Wind Tunnel to evaluate several flow conditioner configurations in the settling chamber for tunnel Mach numbers M_{ts} from 0.20 to 0.916. How honeycomb/screen axial location in the settling chamber affected the flow in the upstream part of the contraction-section also was investigated. Turbulence intensity in the octagonal test section was estimated from measured values at the contraction-section entrance.
The results can be summarized as follows:
1. The lowest longitudinal turbulence intensity measured at the contraction-section entrance was 1.2 percent. On the basis of this measured value, turbulence intensity (including all three components) in the test section was estimated to be between 0.10 and 0.20 percent. The flow conditioner configuration in the settling chamber consisted of a honeycomb plus three 34-mesh screens.

2. Adding a fourth 34-mesh screen did not further reduce longitudinal turbulence intensity. This was probably due to acoustical disturbances or inadequate spacing between screens.

3. Adding screens had an adverse effect on the total pressure profile. Total pressure near the centerline of the contraction-section entrance was 0.3 percent below the average total pressure at $M_{ts} = 0.80$. The adverse effect probably was due to bending of the screens.

4. The flow conditioner configuration consisting of a honeycomb plus three 34-mesh screens resulted in a total pressure loss of about 2.4 times the upstream dynamic pressure for M_{ts} of 0.60 and above.

5. Although the contraction section was quite short for the amount of area ratio reduction, no boundary layer separation was evident over the entire range of tunnel Mach numbers investigated. This was true for the empty settling chamber as well as when honeycomb/screen configurations were installed.

6. The wall Mach number distribution in the upstream part of the contraction section was not significantly affected by the axial location of the honeycomb/screen configuration.

Lewis Research Center
National Aeronautics and Space Administration
Cleveland, Ohio, December 17, 1986

Appendix — Evaluation of Unconventional Flow Conditioner Configurations

As mentioned in the section Apparatus and Procedure, some flow conditioner configurations were installed in the spool section and consequently would not be part of the full-size AWT. However, they would be candidates for use in the 0.1-scale model of the high-speed leg if consideration were given to using this leg as a wind tunnel facility in and of itself. Moreover, these configurations represent an unconventional method for attempting to simultaneously provide a uniform velocity profile and suppress turbulence, and no information has been published on their efficacy for achieving this. Thus these configurations are evaluated in this appendix.

The two flow conditioner configurations (configurations 10 and 11) are shown in figure 30 along with configuration 1, the baseline configuration previously shown in figure 13 and used for comparison.

Configuration 10 was suggested by Dr. Hassan M. Nagib of the Illinois Institute of Technology, who presented a 1-day seminar at NASA Lewis on the technique of simultaneously reducing turbulence and spatial variation in the mean flow by the use of compact honeycomb/screen configurations. It consisted of a 1-mesh grid installed in the upstream part of the spool section and the honeycomb with a 34-mesh exit plane screen installed in the downstream part of the settling chamber. The purpose of the 1-mesh grid was to produce a net increase in turbulence, cause a vigorous mixing of the flow, and thus reduce the mean flow nonuniformities. The distance required for this to be achieved is between 20 and 40 mesh lengths, according to Dr. Nagib. The resulting uniform flow entered the honeycomb, which suppressed principally the transverse components of turbulence. The flow then entered the screen, which not only suppressed the longitudinal component of the upstream turbulence but also modified the turbulence generated by the honeycomb and thus increased the decay rate of the honeycomb-generated turbulence.

Configuration 10 reduced the turbulence from 3.6 to 2.5 percent (fig. 31)—not as much as the conventional flow conditioner, which reduced the turbulence to 1.2 percent (fig. 17). Some additional turbulence reduction could have been achieved by using a 10-mesh rather than the 34-mesh exit plane screen, as discussed in the section Results and Discussion. With the honeycomb/screen removed so that only the 1-mesh grid remained (configuration 11 in fig. 30) the turbulence intensity was 2.9 percent. This was less than the empty spool section/settling chamber value of 3.6 percent, and thus the grid was not a net producer of turbulence.

The grid did not seem to contribute to the reduction in longitudinal turbulence intensity when used in combination with the honeycomb/screen. As shown in figure 21(a) the honeycomb/screen combination installed in the downstream part of the settling chamber (configuration 7 in fig. 13) resulted in a turbulence of 2.6 percent. This was essentially the same value as that for configuration 10.

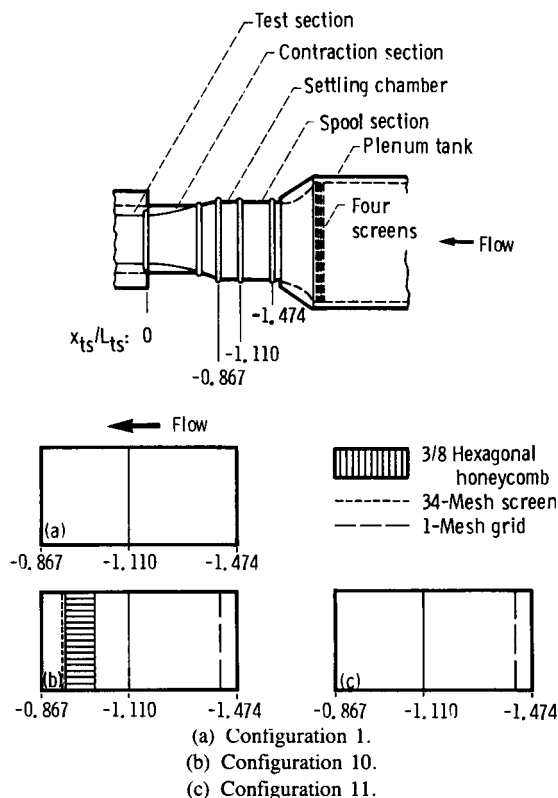As with configurations 2 to 6 (fig. 18) the total pressure

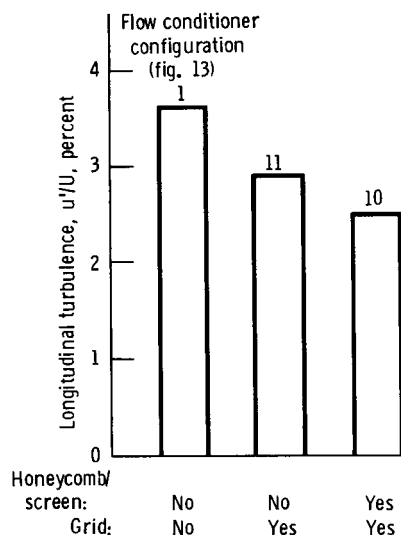Figure 30.—Flow conditioner configurations tested in spool section/settling chamber.

(a) Configuration 1.
(b) Configuration 10.
(c) Configuration 11.

Figure 31.—Effection on longitudinal turbulence at contraction-section entrance of grid alone and in combination with honeycomb screen.

loss coefficient for the two configurations (fig. 32) decreased sharply with increasing tunnel Mach number to $M_{ts} = 0.40$ and then remained essentially constant with further increases in Mach number. For a given M_{ts} the lower loss coefficient occurred when only the grid was installed. At $M_{ts} = 0.80$ the
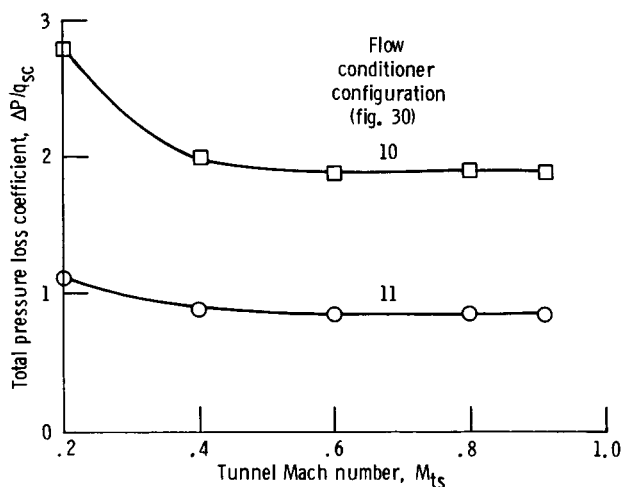
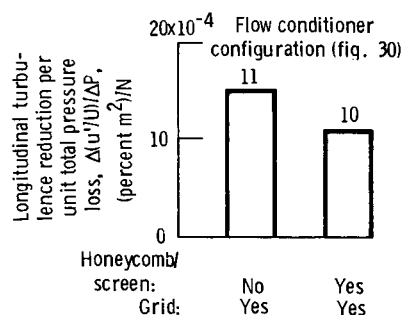Figure 32.—Total pressure loss coefficient across grid alone and in combination with honeycomb screen.

Figure 33.—Effectiveness at contraction-section entrance of grid alone and in combination with honeycomb/screen.

total pressure loss across the grid alone was about 0.85 times the dynamic pressure. This was just a little less than the total pressure loss across the honeycomb with a 34-mesh exit plane screen (configuration 3 in fig. 18). Thus the grid total pressure loss was essentially equivalent to that of a honeycomb/screen. The total pressure loss across the grid plus the honeycomb/screen (configuration 10) was about twice that of just the grid, as expected.

As shown in figure 33 the 1-mesh grid alone was somewhat more effective than the grid plus the honeycomb/screen $(15 \times 10^{-4}$ vs. 11×10^{-4} (percent m^2)/N). The low effectiveness of the grid plus honeycomb/screen was due entirely to the grid, which increased the total pressure loss without reducing the turbulence. The grid alone, however, still was not very effective. Its total pressure loss, as just mentioned, was essentially equivalent to that of a honeycomb/screen. But it was less effective than a honeycomb/screen $(15 \times 10^{-4}$ vs. 27×10^{-4} (percent m^2)/N) because the turbulence reduction was less.

Installing only the 1-mesh grid had a beneficial effect on the total pressure ratio profile of the empty spool section over the entire tunnel Mach number range (fig. 34). The principal effect was to produce a somewhat flatter profile. There are two possible reasons for this: (1) the grid caused considerable mixing of the flow despite not producing a net increase in turbulence; (2) the grid, having relatively large-diameter wires (0.572 cm vs. 0.0168 cm for a 34-mesh screen), deflected less than the screen.

Installing the honeycomb/screen downstream of the 1-mesh grid (configuration 10) had an adverse effect on the total pressure ratio profile at the higher tunnel Mach numbers. The principal effect was to reduce the total pressure near the center of the settling chamber. At $M_{ts} = 0.80$, for example, the total pressure was about 0.2 percent below the average total pressure as compared with essentially average total pressure when only the one 1-mesh grid was installed. Thus the essentially flat total pressure profile that resulted when only the grid was installed was negated when the honeycomb/screen was also installed, probably because of bending of the exit plane screen.
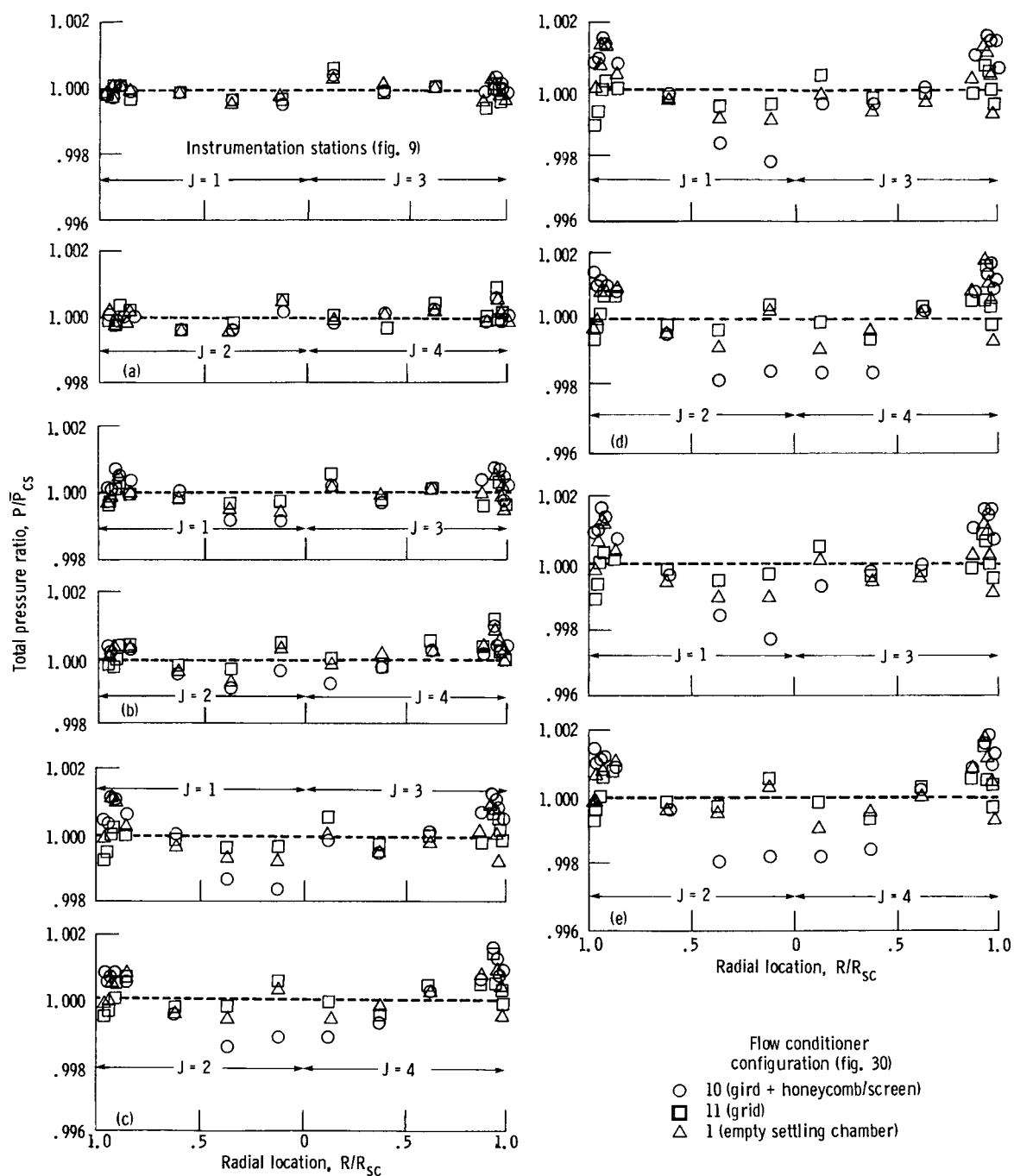
25

Figure 34.—Effect on total pressure ratio at contraction-section entrance of grid alone and in combination with honeycomb/screen.

References

1. Miller, B.A.; and Chamberlin, R.: Altitude Wind Tunnel (AWT)—A Unique Facilty for Propulsion System and Adverse Weather Testing. AIAA Paper 85-0314, Jan. 1985.

2. Blaha, B.; and Shaw, R.J.: The NASA Altitude Wind Tunnel: Its Role in Advanced Icing Research and Development. AIAA Paper 85-0090, Jan. 1985.

3. Abbott, J.M., et al.: Analytical and Physical Modeling Program for the NASA Lewis Research Center's Altitude Wind Tunnel (AWT). AIAA Paper 85-0379, Jan. 1985.

4. Towne, C.E., et al.: Analytical Modeling of Circuit Aerodynamics in the New NASA Lewis Altitude Wind Tunnel. AIAA Paper 85-0380, Jan. 1985.

5. Corsiglia, V.R.; Olson, L.E.; and Falarski, M.D.: Aerodynamic Characteristics of the New 40- by 80-/80- by 120-Foot Wind Tunnel at NASA Ames Research Center. AIAA Paper 84-0601, Mar. 1984.

6. Van Ditshuizen, J.C.A.: Design and Calibration of the 1/10th Scale Model of the NLR Low Speed Wind Tunnel LST 8×6. Wind Tunnel Design and Testing Techniques, AGARD CP-174, AGARD, France, 1975, pp. 8-1 to 8-15.

7. Ciepluch, C.C., et al.: Progress in the Lewis Research Center Altitude Wind Tunnel (AWT) Modeling Program. AIAA 14th Aerodynamic Testing Conference, AIAA, 1986, pp. 183-192.

8. Gelder, T.F., et al.: Wind Tunnel Turning Vanes of Modern Design. AIAA Paper 86-0044, Jan. 1986.

9. Moore, R.D.; Boldman, D.R.; and Shyne, R.J.: Experimental Evaluation of Two Turning Vane Designs for High-Speed Corner of 0.1-Scale Model of NASA Lewis Research Center's Proposed Altitude Wind Tunnel. NASA TP-2570, 1986.

10. Boldman, D.R.; Moore, R.D.; and Shyne, R.J.: Experimental Evaluation of Two Turning Vane Designs for Fan Drive Corner of 0.1-Scale Model of NASA Lewis Research Center's Proposed Altitude Wind Tunnel. NASA TP-2646, 1987.

11. Gelder, T.F.; Moore, R.D.; Shyne, R.J.; and Boldman, D.R.: Experimental Evaluation of Turning Vane Designs for High-Speed and Coupled Fan-Drive Corners of 0.1-Scale Model of NASA Lewis Research Center's Proposed Altitude Wind Tunnel. NASA TP-2681, 1987.

12. Harrington, D.E.; Burley, R.R.; and Corban, R.R.: Experimental Evaluation of Wall Mach Number Distributions of the Octagonal Test Section Proposed for NASA Lewis Research Center's Altitude Wind Tunnel. NASA TP-2666, 1986.

13. Sandborn, V.A.: Resistance Temperature Transducers. Metrology Press, 1972.

14. Bradshaw, P.; and Pankhurst, R.C.: The Design of Low-Speed Wind Tunnels. Progress in Aeronautical Sciences, Vol. 5, D. Keuchemann and L.H.G. Sterne, eds., Pergamon, 1964, pp. 1-69.

15. Schubauer, G.B.; Spangenberg, W.G.; and Klebanoff, P.S.: Aerodynamic Characteristics of Damping Screens. NACA TN-2001, 1950.

16. Tan-Atichat, J.; Nagib, H.M.; and Loehrke, R.I.: Interaction of Free-Stream Turbulence with Screens and Grids: A Balance Between Turbulence Scales. J. Fluid Mech., vol. 114, Jan. 1982, pp. 501-528.

17. Loehrke, R.I.; and Nagib, H.M.: Experiments on Management of Free-Stream Turbulence. AGARD R-598, AGARD, France, 1972.

18. Scheiman, J.: Considerations for the Installation of Honeycomb and Screens to Reduce Wind Tunnel Turbulence. NASA TM-81868, 1981.

19. Scheiman, J.; and Brooks, J.D.: Comparison of Experimental and Theoretical Turbulence Reduction from Screens, Honeycomb, and Honeycomb/Screen Combinations. AIAA 11th Aerodynamics Testing Conference, AIAA, 1980, pp. 129-137.

20. Mehta, R.D.: Turbulent Flow Through Screens. AIAA Paper 84-0538, Jan. 1984.

21. Chmielewski, G.E.: Boundary Layer Considerations in the Design of Aerodynamic Contractions. J. Aircr., vol. 11, no. 8, Aug. 1974, pp. 435-438.

22. Batchelor, G.K.; and Proudman, I.: The Effect of Rapid Distortion of a Fluid in Turbulent Motion. Quart. J. Mech. Appl. Math., vol. 7, pt. 1, 1954, pp. 83-103.

23. Harvey, W.D.; Stainback, P.C.; and Owen, F.K.: An Evaluation and Assessment of Flow Quality in Selected NASA Wind Tunnels. NASA TM-85659, 1983.

24. Tan-Atichat, J.; Nagib, H.M.; and Drubka, R.E.: Effects of Axisymmetric Contractions on Turbulence of Various Scales. (R80-1, Illinois Institute of Technology; NASA Grant NSG-3220) NASA CR-165136, 1980.

1. Report No. NASA TP-2692	2. Government Accession No.	3. Recipient's Catalog No.
4. Title and Subtitle Experimental Evaluation of Honeycomb/Screen Configurations and Short Contraction Section for NASA Lewis Research Center's Altitude Wind Tunnel		5. Report Date May 1987
		6. Performing Organization Code 505-62-3A
7. Author(s) Richard R. Burley and Douglas E. Harrington		8. Performing Organization Report No. E-3142
		10. Work Unit No.
9. Performing Organization Name and Address National Aeronautics and Space Administration Lewis Research Center Cleveland, Ohio 44135		11. Contract or Grant No.
		13. Type of Report and Period Covered Technical Paper
12. Sponsoring Agency Name and Address National Aeronautics and Space Administration Washington, D.C. 20546		14. Sponsoring Agency Code

15. Supplementary Notes

16. Abstract

An experimental investigation was conducted in the high-speed leg of the 0.1-scale model of the proposed Altitude Wind Tunnel to evaluate flow conditioner configurations in the settling chamber and their effect on the flow through the short contraction section. The lowest longitudinal turbulence intensity measured at the contraction-section entrance, 1.2 percent, was achieved with a honeycomb plus three fine-mesh screens. Turbulence intensity in the test section was estimated to be between 0.1 and 0.2 percent with the honeycomb plus three fine-mesh screens in the settling chamber. Adding screens, however, adversely affected the total pressure profile, causing a small defect near the centerline at the contraction-section entrance. No significant boundary layer separation was evident in the short contraction section.

17. Key Words (Suggested by Author(s)) Turbulence reduction; Flow conditioners; Wind tunnel; Screens; Honeycomb; Axisymmetric contractions	18. Distribution Statement Unclassified – unlimited STAR Category 09		
19. Security Classif. (of this report) Unclassified	20. Security Classif. (of this page) Unclassified	21. No of pages 29	22. Price* A03